AUT Journal of Mechanical Engineering

AUT J. Mech. Eng., 7(1) (2023) 19-40
DOI: 10.22060/ajme.2022.21384.6034

Investigation on performance improvement of a fully-actuated quadrotor

Yalda Aslani Darandashi [1], Rasul Fesharakifard [2*], Abdolreza Ohadi [1]

[1] Department of Mechanical Engineering, Amirkabir University of Technology, Tehran, Iran
[2] Department of Textile Engineering, Amirkabir University of Technology, Tehran, Iran

ABSTRACT: Quadrotors provide exclusive performances like vertical landing and taking off, load carrying capacity, and possibility of remote control. A pertinent deficiency of them however concerns their underactuated configuration, which is one of the inherent characteristics of these robots. A dependency between different movements of quadrotor is unavoidable due to this characteristic. To eliminate the dependencies between linear and rotational motions and so increase the number of controllable degrees of freedom, a novel configuration has been presented for the fully-actuated quadrotor. The rotors have the ability to rotate around two perpendicular directions and two degrees of freedom have been added to the system. The motion dependencies between linear and angular degrees are omitted. To investigate the capability of the fully-actuated quadrotor, the novel configuration is introduced and the capabilities of this configuration in eliminating movement dependencies are discussed. To this end, after extracting the motion equations governing the fully-actuated quadrotor using Newton-Euler method and applying a proportional-derivative controller to the model, the performance of this configuration in eliminating the motion dependencies is compared against a conventional underactuated type. It is shown that this configuration is capable of eliminating motion dependencies to a great extent within various simulation results. Finally, by designing a back-stepping controller and applying different trajectories to the proposed fully-actuated quadrotor, its motion capabilities and limitations are thoroughly investigated.

Review History:

Received: May, 20, 2022
Revised: Oct. 25, 2022
Accepted: Nov. 15, 2022
Available Online: Dec. 07, 2022

Keywords:

Quadrotor
Fully-actuated quadrotor
Underactuated quadrotor
proportional-derivative controller
Back-stepping control

1- Introduction

The unique performances of quadrotors, including the ability of vertical landing and taking off, load carrying capacity, and possibility of remote control, have increased their applications worldwide. Their applications include military missions [1], load transportation [2], mapping to supporting rescue operations [3], remote sensing of decks on concrete bridges using thermography infrared [4], surveillance and inspection [5], imaging the forests [6], and examining products with ultrasonic sensors (precision agriculture) [7]. Moreover, by connecting the drones to software applications on smartphones, these devices c-ould be used for video recording and mission planning [8,9].

One of the important issues addressed in research on quadrotors, is the study of the effects of changing the quadrotors configuration on their motional abilities. For instance, in [10], drones with rotating wings, that use a combination of blade-wing mechanism, are designed to benefit from the advantages of fixed-wing drones and quadrotors, simultaneously. These drones act like fixed-wing drones while the wings are in vertical status. However, with a 90-degree rotation of the wings, they will work similar to quadrotors.

In [11] and [12], form-changing multi-rotors were designed to overcome the limitations imposed to quadrotors from the environment. When faced with obstacles, and after identifying them, these multi-rotors continue their path by changing the form, the size or the angle of arms, so that they can avoid any collision with the obstacles.

In normal quadrotors, which are known as underactuated quadrotors, since the number of their control inputs is less than their degrees of freedom, it is not possible to control all degrees of freedom simultaneously, and some degrees of freedom become interdependent [13]. Also, according to previous studies, in the case that the number of rotors increases, for example in hexarotors, motion dependency remains because the rotors are placed in one plane or in the parallel planes. One way to overcome this motion dependency, is to add one or two degrees of freedom to the rotors, in form of rotational ability along one or two axes through servo motor actuators and applying constraints to equalize the number of control inputs and degrees of freedom [14]. In such case, the quadrotor is called a fully-actuated quadrotor.

For example, an H-shaped quadrotor with all its arms capable of simultaneously rotating around their axes, is proposed in [15]. Adding these degrees of freedom to the rotors, resolves the issue of couplings between rotational and translational motions. Since there are 5 control inputs in this

*Corresponding author's email: fesharaki@aut.ac.ir

quadrotor, the control of angles, height and forward speed has been done using a PID controller. Moreover, in [16], a quadrotor with each of its rotors capable of rotating along a separate direction is proposed, and it is shown that adding a fixed wing to the body, reduces the energy consumption and increases system efficiency. Another fully-actuated multi-rotor is called Voliro robot and characterized in [17]. Similar to the previous quadrotor, this hexa-rotor has one degree of freedom for each rotor, and each rotor is capable of rotating about the arm axis. This flying object is used for inspection and imaging in complex environments. Another mode considered for rotation of the rotors is inward or outward rotation. This configuration was first proposed in [18]. It is assumed in this drone, that the angles of the rotors are pairwise equal, moreover a PID controller is used to control the position and angles of this quadrotor. The simulation results show complete elimination of motion couplings between the position and roll and pitch angles. The last case of fully-actuated quadrotors, where each rotor has an additional degree of freedom, is introduced in [19]. In this quadrotor, which is the result of a doctoral dissertation in MIT, changes in the angle of attack of the propellers, made by a mechanism that works similar to the swash plates of helicopters using a servo-motor, are proposed instead of rotations of the rotors.

The second group of fully-actuated quadrotors, are those with each of their rotors having two additional degrees of freedom. One way to increase the number of control inputs in quadrotors is to rotate each of the rotors about the quadrotor arm itself, inwards or outwards [20]. However, adding these two degrees of freedom to each of the rotors, increases the total number of control inputs to 12, and then in order to reduce this number to 6, the angles of all rotors are assumed to be equal along both directions. With this change in quadrotor configuration, the couplings between translational and rotational motions are also eliminated and the addition of two control inputs to the quadrotor, will make it fully-actuated. A novel configuration is proposed in [21], where the rotors are capable of rotating inwards and outwards, as well as rotating parallel to the quadrotor body (along the axis perpendicular to the body). A robot named ALIV3 is introduced in [22]. By two arms, this quadrotor is capable to rotate two of its rotors around two directions, while the other rotors are placed on fixed arms. Moreover, a multi-rotor with four rotors is presented in [23] where the rotors are pairwise coaxial and each two rotors are capable of rotating about two different directions; this configuration is controlled using feedback linearization.

In this article, the advantages and motion capabilities of a fully-actuated quadrotor whose rotors can simultaneously rotate along the y-axis connected to the body and the x-axis connected to the rotor, are investigated. Despite advantageous aspects of performance of a fully-actuated quadrotor which are mentioned above, few studies concentrated on control design for this uncommon configuration. To this end, in section 2, first the coordinate systems (frames) are introduced and then the novel quadrotor configuration under study is presented and after studying the forces and torques applied to this system, and stating the assumptions governing the problem, the dynamic equations of this quadrotor are derived using Newton-Euler method. Once the dynamic is extracted, the next step of design which concerns to study the difference between the application of linear and nonlinear controllers. First the equations are linearized in section 3 and a proportional-derivative controller is designed. In section 4, a back-stepping nonlinear controller is proposed and the controlled system asymptotic stability is guaranteed in theory and by simulation. The simulation results performed by Simulink software are presented in section 5 for both conventional and novel quadrotors. In addition, multiple different scenarios are considered for quadrotor trajectory tracking, and the capabilities of the proposed configuration are shown using the nonlinear controller.

2- Dynamic Modeling

In this section, dynamic governing equations of a fully-actuated quadrotor are derived using the Newton-Euler method. For this purpose, the coordinate systems used in dynamic analysis are first introduced and the transformation matrices between them are defined; then the proposed configuration is discussed in more detail and some Fig.s are also demonstrated. Afterwards, the assumptions of the problem and description of the forces and torques applied to the quadrotor are elaborated and lastly the dynamic equations of the quadrotor are derived.

2- 1- Frames

Since the quadrotor rotors may have an angle to the body and the body may in turn have an angle to the ground, four frames connected to the rotors, $o_i x_i y_i z_i$, and one coordinate system on the body, $oxyz$, are chosen. These frames are illustrated in Fig. 1.

The transformation matrices from the body frame to base frame and from the frames attached to each rotor to the body frame, are calculated in Eqs. (1) and (2), respectively [24].

$$R_B^E = R_{O'X'Y'Z'}^{OXYZ} R_{O''X''Y''Z''}^{O'X'Y'Z'} R_{oxyz}^{O''X''Y''Z''} = \begin{bmatrix} C\psi C\theta & -S\psi C\phi + C\psi S\theta S\phi & S\psi S\phi + C\psi S\theta C\phi \\ S\psi C\theta & C\psi C\phi + S\psi S\theta S\phi & -C\psi S\phi + S\psi S\theta C\phi \\ -S\theta & C\theta S\phi & C\theta C\phi \end{bmatrix} \quad (1)$$

$$R_{r_i}^B = R_{y,\theta_i} R_{x_i',\phi_i} = \begin{bmatrix} C\theta_i & S\phi_i S\theta_i & C\phi_i S\theta_i \\ 0 & C\phi_i & -S\phi_i \\ -S\theta_i & C\theta_i S\phi_i & C\phi_i C\theta_i \end{bmatrix} \quad (2)$$

2- 2- Introducing the proposed configuration

The novel configuration used in this article, is an H-shaped quadrotor whose rotors rotate simultaneously and with the same angles around two different directions about y-axis attached to the body and x-axis connected to the rotor. Figs. 2 and 3 in the following illustrate the y-axis of the body and the x-axis of the rotors, and the sense of rotation of rotors about those axes.

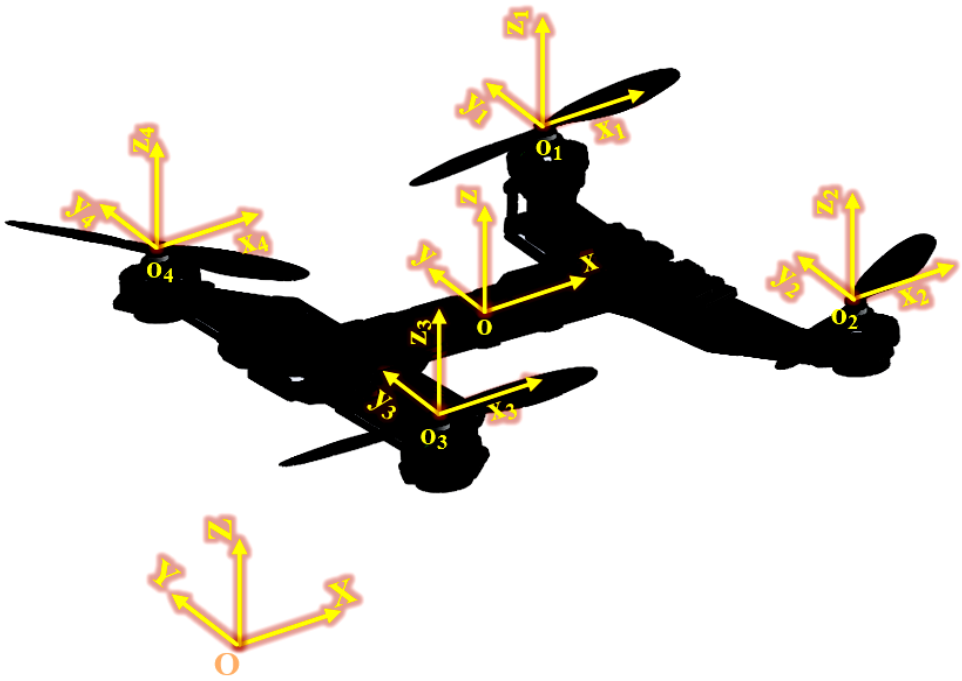

Fig. 1. Base frame, body frame and frames of the rotors.

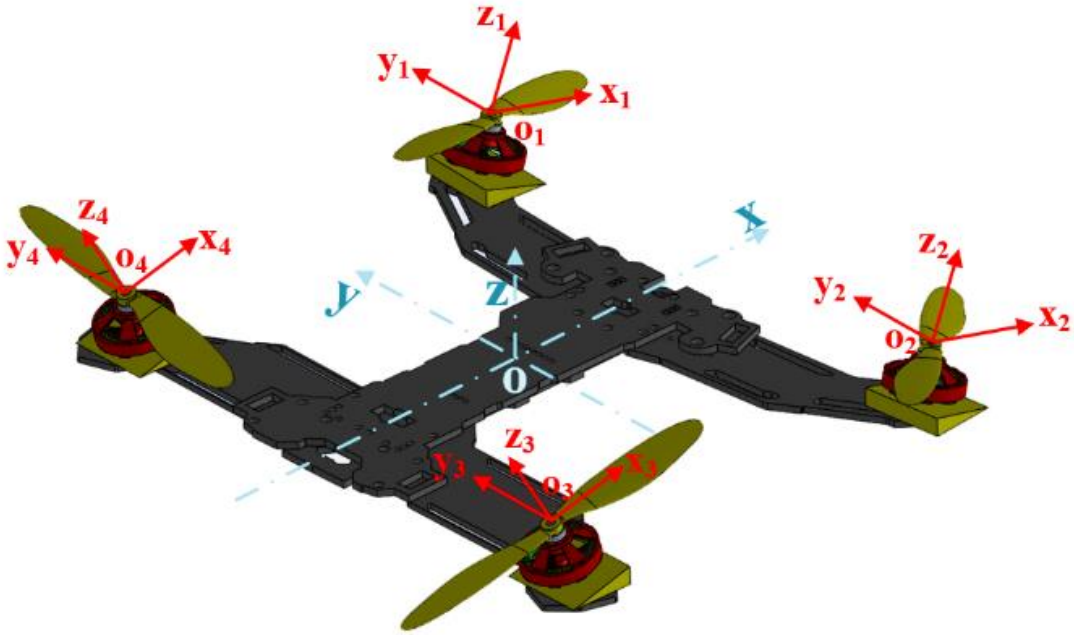

Fig. 2. A fully-actuated quadrotor while the rotors rotate around y-axis of the body frame.

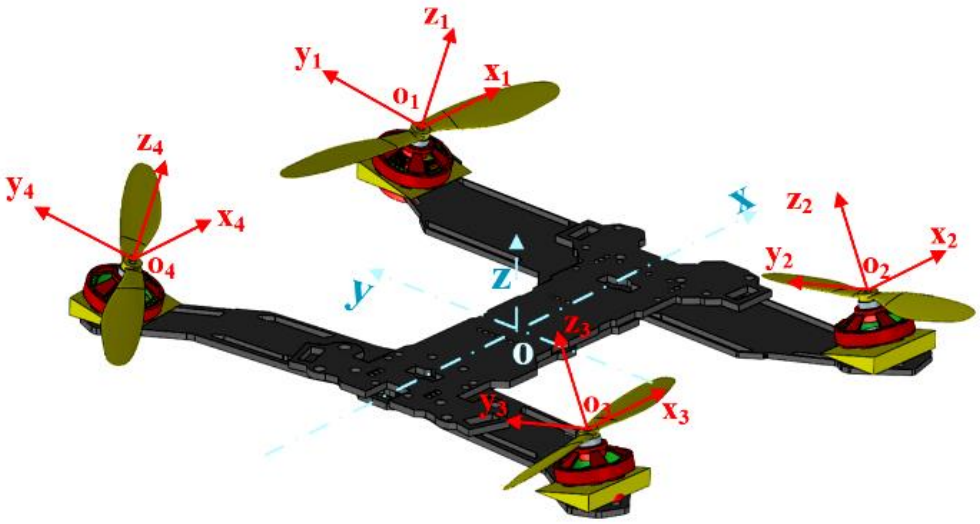

Fig. 3. A fully-actuated quadrotor while the rotors rotate around x-axis of the rotors frames.

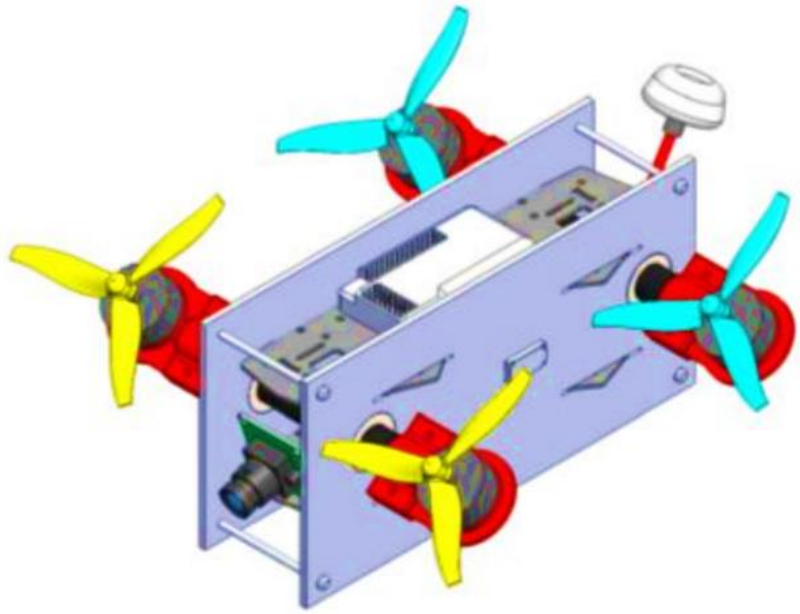

Fig. 4. Quadrotor with H-shaped structure, four rotors tilt synchronously [15]

Servo motors can be used to provide the two degrees of freedom on each of the rotors. However, this article proposes to add two degrees of freedom to rotors and the structural details and mechanism design are not demonstrated. Figs. 4 and 5 give an overall detailed design of the structure. In Fig. 4, a structure for the simultaneous rotation of rotors in one direction for H-shaped quadrotor is presented [15]. Fig. 5 introduces a mechanism for rotating each rotor in two perpendicular directions [22].

Fig. 5. Quadrotor with two degrees of freedom on two rotors [22]

2- 3- Assumptions and applied forces and torques

For dynamical analysis of this fully-actuated quadrotor, the quadrotor is first divided into five rigid bodies. The forces applied to the quadrotor include the thrust, weight, air resistance, and hub forces. Moreover, the drag torque, gyroscope effect, air resistance, and roll torque are the torques applied to the quadrotor frame.

Due to the small linear velocity of the quadrotor, the hub force and the roll torque which are generated as a result of the difference between the relative velocity of air in the propeller blades, are not taken into consideration. Furthermore, the forces and torques resulting from air resistance, which are exerted on the quadrotor due to its linear and angular movements, are neglected. Also, the center of gravity and the geometric center of the quadrotor are assumed to coincide.

The rate of changes in rotor velocities is further assumed to be very high, thus the differential dynamic equations governing the rotors velocities, are not considered in quadrotor equations and it is assumed that the rotors' angular velocities achieve their desired values without any time delays.

This article deals with the conceptual design of the fully-actuated quadrotor. The differential equations governing the actuators that adjust the angles of the rotors about the y-axis attached to the body, the x-axis attached to the rotor, the saturation and other limits of these actuators are neglected. The symmetrical torques that should be excreted to the rotors in order to change their angles, are applied to quadrotor's body as a disturbance.

In addition to the abovementioned parameters, the aerodynamic effects of the rotation of rotors, which are applied by creating overlaps among the rotors and applying a coefficient in the lift force constant, are not taken into consideration. It should be noted that this effect would be negligible if the rotors are placed at an appropriate distance from each other [25].

The thrust force vector, which is generated by the rotors' propeller movements and applied to the quadrotor in upward direction and perpendicular to the propeller movement plane (along the z_i direction of each rotor), is calculated from Eq. (3) in the coordinate system attached to the rotor [26].

$$\vec{T}_i = \begin{bmatrix} 0 & 0 & k_L \omega_i^2 \end{bmatrix}^T \quad , \quad i = 1,2,3,4 \tag{3}$$

In this equation, k_L is a positive lift constant, calculated based on the theories of blade element and motion size, and ω_i denotes the rotor's angular velocity along the z_i-axis.

Since the point that the lift forces are applied to does not coincide with the quadrotor's center of gravity (the torques are written about the quadrotor's center of gravity), each of these forces create a torque about quadrotor's center of gravity. This torque is obtained from the cross product of the vector connecting the center of gravity to the point that the lift force is applied, to the lift force itself. The equations for calculating this torque separately for each of the rotors, are introduced in part 2.4.

The drag torque, which is caused by movements of the rotor propellers, about the axis perpendicular to the plane of the propeller movement and in its opposite direction (about the z_i-axis of each of the rotors), is applied to the quadrotor. The drag torques, stated in the frames attached to each of the rotors, are calculated from Eq. (4) [26].

$$\vec{\tau}_i = \begin{bmatrix} 0 & 0 & -k_D \omega_i |\omega_i| \end{bmatrix}^T \quad , \quad i = 1,2,3,4 \tag{4}$$

where k_D is a positive parameter representing the drag constant.

Due to the fact that the amount of angular motion is stated in the body frame, when taking the derivative of the angular motion, the derivative resulting from the change in the direction of the body system should also be considered along its derivative in the body frame; this derivative is called body gyroscopic effect. This is shown in Eq. (5) [27, 28].

$$\frac{d}{dt}\left(\vec{H}_B\right)_{XYZ} = I\dot{\vec{\Omega}} + \vec{\Omega}\times I\vec{\Omega} \tag{5}$$

In this equation, $\vec{\Omega}$ denotes quadrotor's vector of angular velocity in the body frame, defined by Eq. (6).

$$\vec{\Omega} = \begin{bmatrix} p & q & r \end{bmatrix}^T \tag{6}$$

Moreover, $\left(\vec{\mathrm{H}}_B\right)_{XYZ}$ represents the angular momentum (whose components are written in the body frame), with the value $I\vec{\Omega}$,, where I is defined in the body frame.

2- 4- Complete model

To derive the kinematic equations, the dynamics of the rotors are first investigated. The linear acceleration of each rotor's center of gravity is calculated using the body acceleration, as shown in Eq. (7).

$$\vec{\mathrm{a}}_{\mathrm{r_i}} = \vec{\mathrm{a}}_{\mathrm{CG}} + R_B^E\left[\dot{\vec{\Omega}}\times\vec{\mathrm{r}}_{\mathrm{i}} + \vec{\Omega}\times\left(\vec{\Omega}\times\vec{\mathrm{r}}_{\mathrm{i}}\right)\right] \tag{7}$$

where $\vec{\mathrm{a}}_{\mathrm{r_i}}$ represents the linear acceleration of the i-th rotor, $\vec{\mathrm{a}}_{\mathrm{CG}}$ is the linear acceleration of the body's center of gravity in the base frame, and $\dot{\vec{\Omega}}$, and $\vec{\Omega}$ denote the angular acceleration and velocity of the body in the body frame, respectively. In addition, R_B^E is the transformation matrix from body frame to the base frame, and $\vec{r}_i$ represents the position vector of the i-th rotor in the body frame.

The forces applied to each of the rotors, include the lift force, weight, and the force exerted from the body to the rotor. Therefore, the linear motion equations of each of the rotors, written in the base frame, are as shown in Eq. (8).

$$m_i\vec{\mathrm{a}}_{\mathrm{r_i}} = R_B^E\left(R_{r_i}^B\begin{bmatrix}0\\0\\k_L\omega_i^2\end{bmatrix} + \vec{\mathrm{F}}_{\mathrm{r_i}}\right) + m_i\begin{bmatrix}0\\0\\-g\end{bmatrix} \tag{8}$$

In this equation, $\mathrm{m_i}$ is the mass of the i-th rotor, $\mathrm{R}_{\mathrm{r_i}}^{\mathrm{B}}$ denotes the transformation matrix from the coordinate system attached to the i-th rotor to the body coordinate system, $\vec{\mathrm{F}}_{\mathrm{r_i}}$ is the force applied to the i-th rotor from the body and g represents the gravity acceleration constant. Moreover, $\mathrm{k_L}$ denotes the lifting constant and ω_{i} is the angular velocity of the i-th rotor. Based on Eq. (8), the force applied from the body to the i-th rotor, can be derived as shown in Eq. (9).

$$\vec{\mathrm{F}}_{\mathrm{r_i}} = \left(R_B^E\right)^T\left(m_i\vec{\mathrm{a}}_{\mathrm{r_i}} + m_i\begin{bmatrix}0\\0\\g\end{bmatrix}\right) - R_{r_i}^B\begin{bmatrix}0\\0\\k_L\omega_i^2\end{bmatrix} \tag{9}$$

In this equation, the force resulting from the acceleration generated in the rotor's center of mass due to its distance to the axis of rotation, which includes vertical and tangential components, is neglected, with the assumption that the axis of rotation passes through the rotor's center of mass.

In order to derive rotational dynamics of the rotor, first the derivative of its angular motion must be calculated. Eqs. (10), and (11), calculate the angular motion of the i-th rotor and its derivative, respectively.

$$\vec{\mathrm{H}}_{\mathrm{i}} = J_i\vec{\omega}_{\mathrm{r_i}} \tag{10}$$

$$\frac{d}{dt}\left(\vec{\mathrm{H}}_i\right)_{XYZ} = \frac{d}{dt}\left(\vec{\mathrm{H}}_i\right)_{x_iy_iz_i} + \vec{\omega}'_{\mathrm{r_i}}\times\left(\vec{\mathrm{H}}_i\right) \tag{11}$$

In these equations, $\vec{\mathrm{H}}_{\mathrm{i}}$ denotes the amplitude of the i-th rotor's angular motion, stated in the coordinate system attached to the same rotor. Moreover, $\mathrm{J_i}$ is the moment of inertia of the rotor, and $\vec{\omega}_{\mathrm{r_i}}$ represent the angular velocity of the i-th rotor, while $\vec{\omega}'_{\mathrm{r_i}}$ is the angular velocity of the coordinate system attached to that rotor. $\vec{\omega}_{\mathrm{r_i}}$ and $\vec{\omega}'_{\mathrm{r_i}}$ are calculated from Eqs. (12) and (13), respectively.

$$\vec{\omega}_{\mathrm{r_i}} = R_{r_i}^{BT}\left(\vec{\Omega} + \begin{bmatrix}0\\\dot{\theta}_i\\0\end{bmatrix}\right) + \begin{bmatrix}\dot{\phi}_i\\0\\\omega_i\end{bmatrix} \tag{12}$$

$$\vec{\omega}'_{\mathrm{r_i}} = (R_{r_i}^B)^T\left(\vec{\Omega} + \begin{bmatrix}0\\\dot{\theta}_i\\0\end{bmatrix}\right) + \begin{bmatrix}\dot{\phi}_i\\0\\0\end{bmatrix} \tag{13}$$

Here, $\vec{\omega}_{\mathrm{r_i}}$ and $\vec{\omega}'_{\mathrm{r_i}}$, which are the angular velocity of the i-th rotor and the coordinate system attached to that rotor, respectively, are state $\dot{\theta}_{\mathrm{i}}$ the coordinate system attached to the rotor. Moreover, $\dot{\theta}_{\mathrm{i}}$ represents the angular velocity of the i-th rotor about the y-axis attached to the body, and $\dot{\phi}_{\mathrm{i}}$ is the angular velocity of this rotor about the x-axis attached to it, and ω_{i} is the angular velocity of the rotor's propeller. By

substituting Eq. (10) in Eq. (11), the derivative of the angular motion is derived as shown in Eq. (14).

$$\frac{d}{dt}\left(\vec{\mathrm{H}}_{\mathrm{i}}\right)_{XYZ} = J_i \dot{\vec{\omega}}_{\mathrm{r_i}} + \vec{\omega}'_{\mathrm{r_i}} \times J_i \vec{\omega}_{\mathrm{r_i}} \tag{14}$$

It should be noted that the derivative of angular motion is taken with respect to the base frame, but stated in the body frame. The $\vec{\omega}'_{\mathrm{r_i}}$ in this equation, is calculated using Eq. (15).

$$\dot{\vec{\omega}}_{\mathrm{r_i}} = \left(R_{r_i}^{B}\right)^{T}\left(\dot{\vec{\Omega}} + \begin{bmatrix} 0 \\ \ddot{\theta}_i \\ 0 \end{bmatrix}\right) + (\dot{R}_{r_i}^{B})^{T}\left(\vec{\Omega} + \begin{bmatrix} 0 \\ \dot{\theta}_i \\ 0 \end{bmatrix}\right) + \begin{bmatrix} \ddot{\phi}_i \\ 0 \\ \dot{\omega}_i \end{bmatrix} \tag{15}$$

The dynamic equation of the rotational movement of the i-th rotor, written in the body coordinate system, is presented in Eq. (16).

$$R_{r_i}^{B}\left(J_i \dot{\vec{\omega}}_{\mathrm{r_i}} + \vec{\omega}'_{\mathrm{r_i}} \times J_i \vec{\omega}_{\mathrm{r_i}}\right) = \vec{\tau}_{\mathrm{r_i}}^{\mathrm{B}} + R_{r_i}^{B}\begin{bmatrix} 0 \\ 0 \\ -k_D \omega_i |\omega_i| \end{bmatrix} \tag{16}$$

In this equation, $\vec{\tau}_{\mathrm{r_i}}^{\mathrm{B}}$ is the vector of torques the body exerts on the rotor, and $\mathrm{k_D}$ is the drag constant. Moreover, the effect of non-coincidence between the center of mass and the connection of the rotors to the body is ignored and the equations are written about the rotor's center of mass.

Finally, using the aforementioned equations, the linear and angular motion equations of the quadrotor are derived as follows.

$$\left(M - \sum_{i=1}^{4} m_i\right)\begin{bmatrix} \ddot{X} \\ \ddot{Y} \\ \ddot{Z} \end{bmatrix} = \left(M - \sum_{i=1}^{4} m_i\right)\begin{bmatrix} 0 \\ 0 \\ -g \end{bmatrix} - R_B^E \sum_{i=1}^{4} \vec{\mathrm{F}}_{\mathrm{r_i}} \tag{17}$$

$$I_B \dot{\vec{\Omega}} = -\vec{\Omega} \times \left(I_B \vec{\Omega}\right) - \sum_{i=1}^{4} \vec{\tau}_{\mathrm{r_i}}^{\mathrm{B}} - \sum_{i=1}^{4} (\vec{\mathrm{r}}_{\mathrm{i}} \times \vec{\mathrm{F}}_{\mathrm{r_i}}) \tag{18}$$

where M is the total mass of the quadrotor, $\begin{bmatrix} \ddot{\mathrm{X}} \\ \ddot{\mathrm{Y}} \\ \ddot{\mathrm{Z}} \end{bmatrix}$ represents the second derivative of the coordinates of the quadrotor in the base frame, and $\mathrm{I_B}$ represents the moment of inertia of the body in the body frame. It should also be noted that Eq. (17) is written with respect to the base frame, while Eq. (18) is written in the body one.

3- Linear controller design

In this section, to design a linear controller for the proposed new configuration, it is assumed that the impacts of the derivatives of angular motion of the rotors are negligible. Considering this assumption and simplifying the model, Eqs. (17) and (18) can be rewritten as Eqs. (19) and (20).

$$M\begin{bmatrix} \ddot{X} \\ \ddot{Y} \\ \ddot{Z} \end{bmatrix} = M\begin{bmatrix} 0 \\ 0 \\ -g \end{bmatrix} + R_B^E \sum_{i=1}^{4} R_{ri}^{B}\begin{bmatrix} 0 \\ 0 \\ k_L \omega_i^2 \end{bmatrix} \tag{19}$$

$$\begin{aligned} I\,\dot{\vec{\Omega}} + \vec{\Omega} \times \left(I\vec{\Omega}\right) = \sum_{i=1}^{4} \Big(& R_{ri}^{B}\begin{bmatrix} 0 \\ 0 \\ -k_D \omega_i |\omega_i| \end{bmatrix} \\ & + \vec{\mathrm{r}}_{\mathrm{i}} \times \left(R_{ri}^{B}\begin{bmatrix} 0 \\ 0 \\ k_L \omega_i^2 \end{bmatrix}\right)\Big) \end{aligned} \tag{20}$$

Due to the similarity of the rotation angles of the rotors, R_{ri}^{B} has the same value for all rotors, and thus Eqs. (19) and (20) can be written as Eqs. (21) and (22), respectively.

$$M\begin{bmatrix} \ddot{X} \\ \ddot{Y} \\ \ddot{Z} \end{bmatrix} = M\begin{bmatrix} 0 \\ 0 \\ -g \end{bmatrix} + R_B^E R_{all\ Rotors}^{B} \sum_{i=1}^{4}\begin{bmatrix} 0 \\ 0 \\ k_L \omega_i^2 \end{bmatrix} \tag{21}$$

$$\begin{aligned} & I\,\dot{\vec{\Omega}} + \vec{\Omega} \times \left(I\vec{\Omega}\right) = \\ & \sum_{i=1}^{4} \Big(R_{all\ Rotors}^{B}\begin{bmatrix} 0 \\ 0 \\ -k_D \omega_i |\omega_i| \end{bmatrix} \\ & \quad + \vec{\mathrm{r}}_{\mathrm{i}} \times \left(R_{all\ Rotors}^{B}\begin{bmatrix} 0 \\ 0 \\ k_L \omega_i^2 \end{bmatrix}\right)\Big) \end{aligned} \tag{22}$$

Defining the virtual control inputs as in Eqs. (23) and (24), and simplifying the equations, the linear and angular motion equations of the quadrotor are derived as in Eqs. (25) and (26).

$$\begin{bmatrix} U_1 \\ U_2 \\ U_3 \end{bmatrix} = R_B^E R_{rall\ Rotors}^B \sum_{i=1}^{4} \begin{bmatrix} 0 \\ 0 \\ k_L \omega_i^2 \end{bmatrix} \tag{23}$$

$$\begin{bmatrix} U_4 \\ U_5 \\ U_6 \end{bmatrix} = \sum_{i=1}^{4} (R_{all\ Rotors}^B \begin{bmatrix} 0 \\ 0 \\ -k_D \omega_i \left|\omega_i\right| \end{bmatrix} + \vec{r}_i \times (R_{all\ Rotors}^B \begin{bmatrix} 0 \\ 0 \\ k_L \omega_i^2 \end{bmatrix})) \tag{24}$$

$$\begin{bmatrix} \ddot{X} \\ \ddot{Y} \\ \ddot{Z} \end{bmatrix} = \begin{bmatrix} 0 \\ 0 \\ -g \end{bmatrix} + \frac{1}{M} \begin{bmatrix} U_1 \\ U_2 \\ U_3 \end{bmatrix} \tag{25}$$

$$\begin{bmatrix} I_{xx}\dot{p} \\ I_{yy}\dot{q} \\ I_{zz}\dot{r} \end{bmatrix} = \begin{bmatrix} (I_{yy} - I_{zz})qr \\ (I_{zz} - I_{xx})pr \\ (I_{xx} - I_{yy})pq \end{bmatrix} + \begin{bmatrix} U_4 \\ U_5 \\ U_6 \end{bmatrix} \tag{26}$$

Eq. (27) is also derived by linearizing Eq. (26).

$$\begin{bmatrix} I_{xx}\dot{p} \\ I_{yy}\dot{q} \\ I_{zz}\dot{r} \end{bmatrix} = \begin{bmatrix} U_4 \\ U_5 \\ U_6 \end{bmatrix} \tag{27}$$

For the sake of designing a proportional-derivative controller, the auxiliary control inputs are defined as stated in Eqs. (28)-(33).

$$U_1 = M\left(k_{p_X} e_X + k_{D_X} \dot{e}_X\right) \tag{28}$$

$$U_2 = M\left(k_{p_Y} e_Y + k_{D_Y} \dot{e}_Y\right) \tag{29}$$

$$U_3 = M\left(g + k_{p_Z} e_Z + k_{D_Z} \dot{e}_Z\right) \tag{30}$$

$$U_4 = I_{xx}\left(k_{p_\phi} e_\phi + k_{D_\phi} \dot{e}_\phi\right) \tag{31}$$

$$U_5 = I_{yy}\left(k_{p_\theta} e_\theta + k_{D_\theta} \dot{e}_\theta\right) \tag{32}$$

$$U_6 = I_{zz}\left(k_{p_\psi} e_\psi + k_{D_\psi} \dot{e}_\psi\right) \tag{33}$$

4- Non-linear controller design

The performance of the linear and back-stepping controller in tracking of a sinusoidal trajectory has been compared for a fully-actuated quadrotor [27]. Based on simulation results, it is demonstrated that in terms of tracking error and time delay, the back-stepping controller is preferable and in this part, a back-stepping controller is developed for a sinusoidal input of the system.

As mentioned in section 2.3, the complete equations governing the fully-actuated quadrotor, are as written in Eqs. (17) and (18). In this section, the virtual control inputs are defined by Eqs. (23) and (24), similar to section 3, and replacing them in Eqs. (17) and (18) will result in final dynamic Eq. (25) and (26).

To design a back-stepping controller, first the differential Eq. (25) and (26) must be transformed into state space format. Considering state variables x_1 to x_{12} as shown in Eqs. (34) and (35), the linear and angular dynamic equations of the fully-actuated quadrotor are derived as in Eqs. (36) and (37).

$$\left[x_1\ .x_2\ .x_3\ .x_4\ .x_5\ .x_6\right] = \left[X\ .\dot{X}\ .Y.\dot{Y}.Z.\dot{Z}\right]^T \tag{34}$$

$$\left[x_7\ .x_8\ .x_9\ .x_{10}\ .x_{11}\ .x_{12}\right] = \left[\phi\ .\dot{\phi}\ .\theta.\dot{\theta}.\psi.\dot{\psi}\right]^T \tag{35}$$

$$\begin{bmatrix}\dot{x}_1\\ \dot{x}_2\\ \dot{x}_3\\ \dot{x}_4\\ \dot{x}_5\\ \dot{x}_6\end{bmatrix}=\begin{bmatrix}x_2\\ \frac{1}{M}U_1\\ x_4\\ \frac{1}{M}U_2\\ x_6\\ -g+\frac{1}{M}U_3\end{bmatrix} \tag{36}$$

$$\begin{bmatrix}\dot{x}_7\\ \dot{x}_8\\ \dot{x}_9\\ \dot{x}_{10}\\ \dot{x}_{11}\\ \dot{x}_{12}\end{bmatrix}=\begin{bmatrix}x_8\\ \frac{\left(I_{yy}-I_{zz}\right)x_{10}x_{12}}{I_{xx}}+\frac{U_4}{I_{xx}}\\ x_{10}\\ \frac{\left(I_{zz}-I_{xx}\right)x_8x_{12}}{I_{yy}}+\frac{U_5}{I_{yy}}\\ x_{12}\\ \frac{\left(I_{xx}-I_{yy}\right)x_8x_{10}}{I_{zz}}+\frac{U_6}{I_{zz}}\end{bmatrix} \tag{37}$$

To track the paths along X, first the error variable along this direction, the first state variable, is defined as Eq. (38), and then the Lyapunov function V_1 for the error variable, e_1, is defined as Eq. (39).

$$e_1=x_{1d}-x_1 \tag{38}$$

$$V_1\left(e_1\right)=\frac{1}{2}e_1^2 \tag{39}$$

The time-derivative of this function is defined in Eq. (40).

$$\dot{V}_1\left(e_1\right)=e_1\left(\dot{x}_{1d}-\dot{x}_1\right) \tag{40}$$

According to Eq. (36), $\dot{x}_1$ is equal to x_2. By substituting this equation into Eq. (40), the derivative of the Lyapunov function, V_1, is calculated as follows:

$$\dot{V}_1\left(e_1\right)=e_1\left(\dot{x}_{1d}-\dot{x}_1\right) \tag{41}$$

Defining x_2 according to Eq. (42), the derivative of the Lyapunov function will be calculated as shown in Eq. (43).

$$x_2=\dot{x}_{1d}+\alpha_1e_1 \quad , \quad \alpha_1>0 \tag{42}$$

$$\dot{V}_1\left(e_1\right)=-\alpha_1e_1^2 \quad , \quad \alpha_1>0 \tag{43}$$

From Eq. (43), assuming α_1 to be positive, $\dot{V}_1$ will be negative except for when $e_1=0$. Thus, the system will be asymptotically stable in $e_1=0$.

In the second stage of the back-stepping controller design, for linear motion along X direction, a Lyapunov function must be defined to stabilize x_2. To this end, first the error variable e_2 is calculated from the following Eq. (44).

$$e_2=x_2-\dot{x}_{1d}-\alpha_1e_1 \tag{44}$$

Defining the Lyapunov function V_2 as in Eq. (45), and then taking its derivative would result in Eq. (46).

$$V_2\left(e_1\ .e_2\right)=\frac{1}{2}\left(e_1^2+e_2^2\right) \tag{45}$$

$$\begin{aligned}&\dot{V}_2\left(e_1\ .e_2\right)=e_1\dot{e}_1+e_2\dot{e}_2=\\ &e_1\dot{e}_1+e_2\left(\dot{x}_2-\ddot{x}_{1d}-\alpha_1\dot{e}_1\right)\end{aligned} \tag{46}$$

By comparing $\dot{e}_1$ with Eq. (44), Eq. (47) is obtained for $\dot{e}_1$. Substituting this equation and the value of $\dot{x}_2$ from Eq. (36) into Eq. (46), and simplifying the result, the derivative of the Lyapunov function $\dot{V}_2$, is obtained as in Eq. (48).

$$\dot{e}_1=-e_2-\alpha_1e_1 \tag{47}$$

$$\begin{aligned}&\dot{V}_2\left(e_1\ .e_2\right)=e_2\left(\frac{1}{M}U_1\right)\\ &-e_2\left(\ddot{x}_{1d}-\alpha_1\left(e_1+\alpha_1e_1\right)\right)-e_1e_2-\alpha_1e_1^2\end{aligned} \tag{48}$$

Defining U_1 according to Eq. (49), the derivative of the Lyapunov function is calculated from Eq. (50). If α_1 and α_2 are negative, then the derivative of the Lyapunov function will be negative and the system will become asymptotically stable at the origin.

$$U_1 = M\left(\ddot{x}_{1d} + e_1 - \alpha_1 \left(e_1 + \alpha_1 e_1 \right) - \alpha_2 e_2 \right) \quad , \ \alpha_1, \alpha_2 > 0 \quad (49)$$

$$\dot{V}_2 \left(e_1 \ . e_2 \right) = -\alpha_1 e_1^2 - \alpha_2 e_2^2 \quad , \ \alpha_1, \alpha_2 > 0 \quad (50)$$

Similar to the motion along X direction, the system will become asymptotically stable along Y and Z axes, by defining the control inputs U_2 and U_3 using Eqs. (51) and (52), respectively.

$$U_2 = M\left(\ddot{x}_{3d} + e_3 - \alpha_3 \left(e_3 + \alpha_3 e_3 \right) - \alpha_4 e_4 \right) \quad , \ \alpha_3, \alpha_4 > 0 \quad (51)$$

$$U_3 = M\left(g + \ddot{x}_{5d} + e_5 - \alpha_5 \left(e_5 + \alpha_5 e_5 \right) - \alpha_6 e_6 \right) \quad , \ \alpha_5, \alpha_6 > 0 \quad (52)$$

Moreover, using the same procedure, control inputs U_4 to U_6, can be defined for the angles ϕ, θ, and ψ as shown in Eqs. (53)-(55).

$$U_4 = I_{xx} \left(-\frac{\left(I_{yy} - I_{zz} \right) x_{10} x_{12}}{I_{xx}} + \ddot{x}_{7d} + e_7 - \alpha_7 \left(e_7 + \alpha_7 e_7 \right) - \alpha_8 e_8 \right) \quad , \ \alpha_7, \alpha_8 > 0 \quad (53)$$

$$U_5 = I_{yy} \left(-\frac{\left(I_{zz} - I_{xx} \right) x_8 x_{12}}{I_{yy}} + \ddot{x}_{9d} + e_9 - \alpha_9 \left(e_9 + \alpha_9 e_9 \right) - \alpha_{10} e_{10} \right) \quad , \ \alpha_9, \alpha_{10} > 0 \quad (54)$$

$$U_6 = I_{zz} \left(-\frac{\left(I_{xx} - I_{yy} \right) x_8 x_{10}}{I_{zz}} + \ddot{x}_{11d} + e_{11} - \alpha_{11} \left(e_{11} + \alpha_{11} e_{11} \right) - \alpha_{12} e_{12} \right) \quad , \ \alpha_{11}, \alpha_{12} > 0 \quad (55)$$

5- Simulation results

In this section, the advantages of the proposed configuration over conventional quadrotors, which include increasing the number of controllable degrees of freedom and elimination of couplings between linear and angular motions, are determined by performing simulations in Simulink environment. Furthermore, motion capabilities of the proposed configuration are demonstrated.

5- 1- Quadrotor specifications

The specifications used in the simulations are presented in Table 1. However, the height of the rotors has been reduced to 0.038 m, the reason of which is explained in section 5.2.

5- 2- Comparison of performance

In this part, the new configuration is compared to the conventional quadrotor by applying the proposed linear controller. During all simulations, the maximum angular velocity of the rotors is supposed equal to 10000 rpm, and the maximum angle for ϕ_{aR} is assumed to be equal to $80°$. In order to show the elimination of couplings between linear and angular movements in the new configuration, step inputs for the angles ϕ and θ are applied separately to the new and conventional quadrotors, and the Y and X position diagrams in terms of time, are investigated for both configurations, respectively. This procedure is also repeated for step inputs to locations along X and Y-axes, and the diagrams of angles ϕ and θ are then studied. In this section, a proportional-derivative controller is used.

When designing the linear controller, the coefficients are manually selected so that the value of overshoot for tracking of angles and positions remains under 17%, and the rise time decreases as much as possible. The amount of error was not considered precisely during the design of controllers, and it was only intended to have an acceptable value at the end of the first 20 seconds of the simulation. These coefficients are presented in Tables 2 and 3, for conventional and new configurations, respectively.

In this section, since the values of $\dot{\theta}_{aR}$, $\dot{\phi}_{aR}$, $\ddot{\theta}_{aR}$, and $\ddot{\phi}_{aR}$ are small and moments of inertia of the rotors are also insignificant compared to the moment of inertia of the quadrotor's body, the impacts of rotors' disturbances, generated during the linear controller design due to the performed simplifications, are negligible and thus have no significant effect on the results.

5- 3- Tracking a step function for the angle ϕ

Fig. 6(a) illustrates the angle ϕ with respect to time, while Fig. 6(b) shows Y with respect to time, for both old and new configurations.

As shown in Fig. 6, the diagrams of ϕ with respect to time for both configurations are overlaid on each other. The reason for this matter is that dynamic equations of angular motion for both configurations, are identical after defining virtual control inputs. In the conventional configuration with deviation of quadrotor along the x-axis attached to the quadrotor, the angle ϕ, the lift forces of the rotors gain components along the Y-axis of the reference coordinate system, and this results in the acceleration of the quadrotor and its movement along this axis. However, in the newly proposed configuration, considering the increase in the

Table 1. Characteristics of the quadrotor used in simulation.

Characteristics	Symbol	Value	Unit
Total mass	M	0.5216	kg
Moment of inertia of quadrotor around x	I_{xx}	0.003331	$kg.m^2$
Moment of inertia of quadrotor around y	I_{yy}	0.003652	$kg.m^2$
Moment of inertia of quadrotor around z	I_{zz}	0.006621	$kg.m^2$
Lift coefficient	k_L	1.503×10^{-6}	$kg.m$
Drag coefficient	k_D	3.341×10^{-8}	$kg.m^2$
Height	h	0.0827	m
Arm length	L	0.106	m
Distance between arms/2	b	0.098	m
Moment of inertia of each rotor around x and y	J_{xx} J_{yy} و	2.013×10^{-6}	$kg.m^2$
Moment of inertia of each rotor around z	J_{zz}	1.077×10^{-5}	$kg.m^2$
Mass of each rotor	m	0.034	kg

Table 2. Control gains used for underactuated quadrotor.

Control gains	k_P	k_D
ϕ	–0.14	–1
θ	–0.14	–1
X	–0.001	–0.88
Y	–0.001	–0.85

Table 3. Control gains used for fully-actuated quadrotor.

Control gains	k_P	k_D
ϕ	–0.14	–2.1
θ	–0.14	–2.1
X	–0.15	–2
Y	–0.15	–2

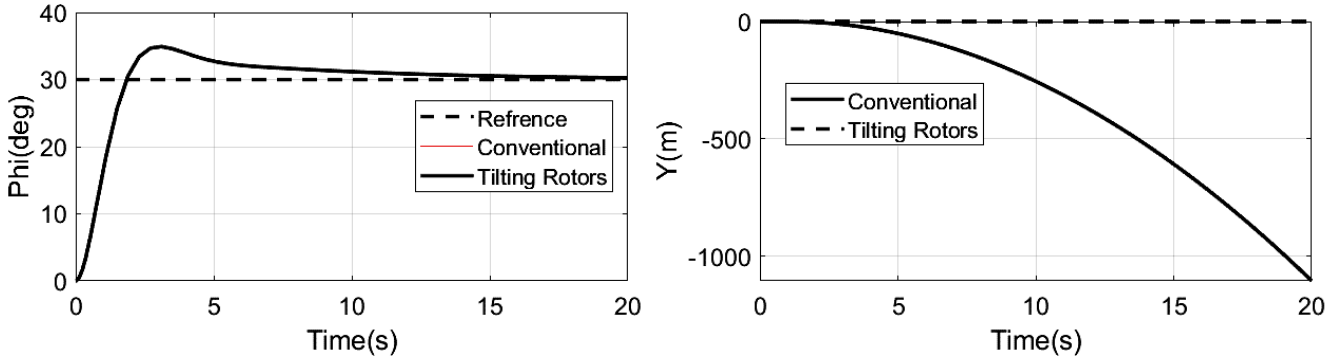

Fig. 6. Motion tracking around ϕ (a) and along Y (b) for conventional and new configurations for step references, while the other axis have no input.

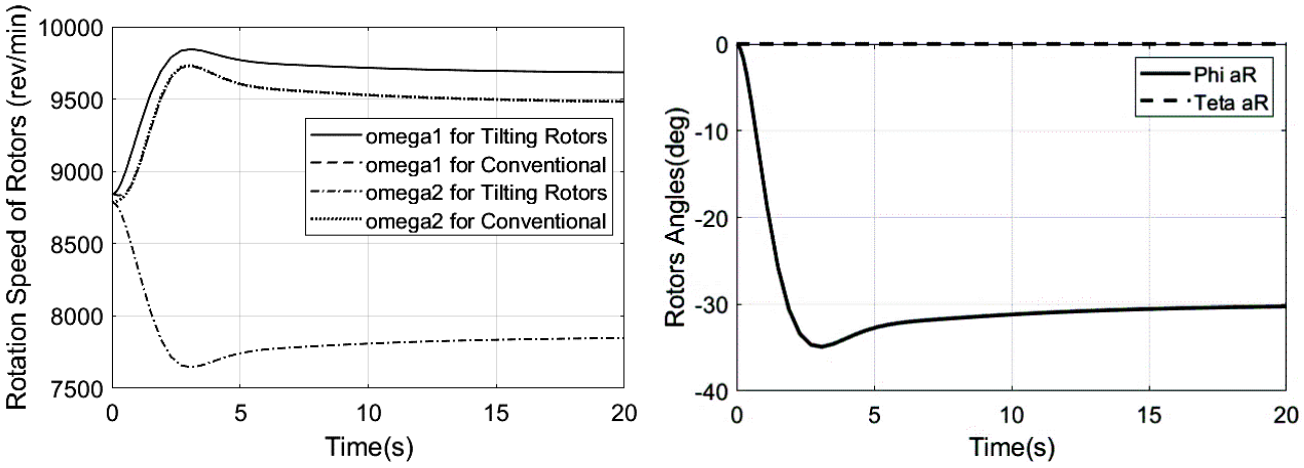

(a) **(b)**

Fig. 7. Diagrams of angular velocities for underactuated and fully-actuated quadrotors and diagrams of angles of the rotors for the fully-actuated quadrotor to follow a step in ϕ while the other degrees have zero references. (a) Angular velocities versus time, (b) Rotors angles for the new configuration versus time.

number of control inputs, apart from applying a step input for the abovementioned angle, a zero input is applied to other degrees of freedom, including the position along the Y-axis. Thus, in this quadrotor, the position along the Y-axis remains at the origin. To this end, the rotors must rotate in a way so that their lift forces does not generate any components along the Y-axis with the rotation of the body and changes in the ϕ angle of the quadrotor, as illustrated in Fig. 7(b). It is seen from this Fig. that all rotors rotate along the x-axis attached to the rotors, in exactly the same motion as the angle ϕ, but with opposite directions, in order to maintain their lift force component along the Y-axis equal to zero.

The angular velocities of rotors 1 and 2 with respect to time are shown in Fig. 7(a) for both configurations. The angular velocities of rotors 3 and 4, are equal to those of rotors 1 and 2, but in opposite directions.

It can be seen from Fig. 7(a) that for the conventional quadrotor, the angular velocities of rotors 1 and 2 are slightly different at the beginning in order to create the torque necessary for changing the angle ϕ, and eventually become equal to each other. However, in the quadrotor with the new configuration, after the angular velocity of ϕ reaches its desired value, the angular velocities of the two rotors remain different from each other. The reason for this is that due to the rotation of rotors in the opposite direction of the quadrotor about the x-axis, their lift forces gain a component along the y-axis and this force creates a torque along the x-axis due to the height of the rotors to the center of gravity. Thus, the angular velocities of rotors 1 and 2 must remain different in order to overcome this torque.

Another issue observed from this plot, is the higher angular velocity of rotors in the conventional quadrotor,

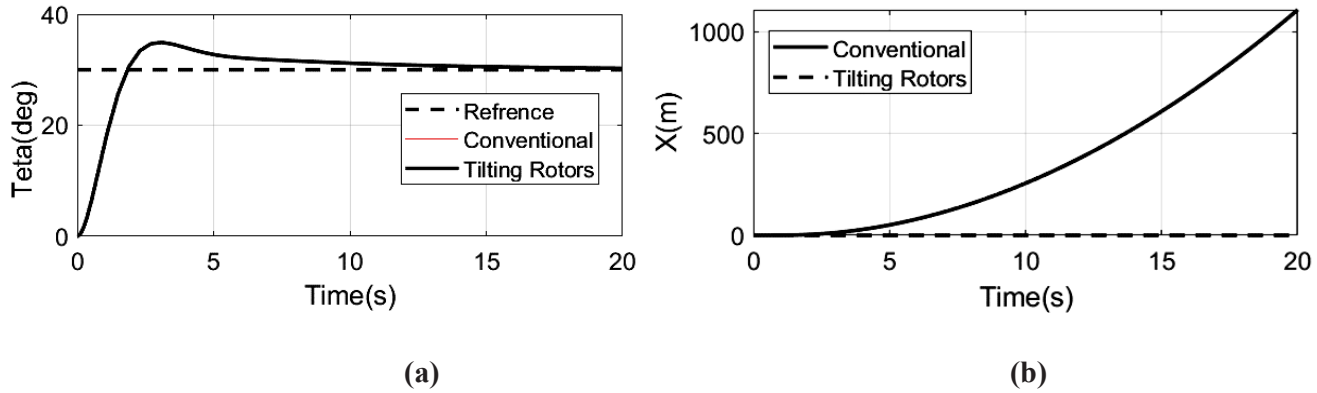

(a) (b)

Fig. 8. Diagrams of angular and linear positions along θ and X for underactuated and fully-actuated quadrotors for following a step in θ while the other degrees have zero references. (a) Angular position of θ versus time, (b) Linear position of X versus time.

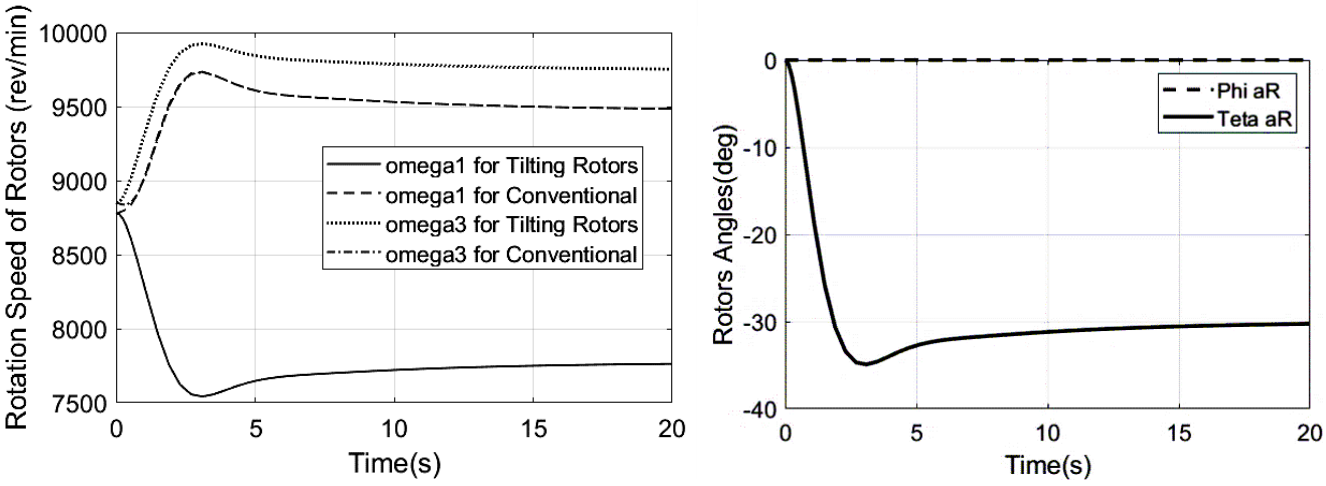

(a) (b)

Fig. 9. Diagrams of angular velocities for underactuated and fully-actuated quadrotors and plots of angles of the rotors for the fully-actuated quadrotor to follow a step in ϕ while the other degrees have zero references. (a) Angular velocities versus time, (b) Rotors angles for the new configuration versus time.

which causes it to consume more energy. This is due to the reduction of vertical component of the rotors' lift forces in this configuration, resulting from the quadrotor body rotation and the need for increasing angular velocity of the rotors and higher energy consumption to overcome the weight force. In the new configuration, since the rotors rotate relative to the body in a way that the direction of their lift forces does not change, there will be no need to increase the created lift force and thus it will experience lower energy consumption.

5- 4- Tracking a step reference for the angle ϕ

The diagram of the angle θ versus time is shown in Fig. 8(a), while Fig. 8(b) presents the changes in X direction, for both new and conventional quadrotors.

The results in this part are similar to tracking a step for the angle ϕ, with the difference that when the conventional quadrotor rotates about the direction of θ, its position changes along the X-axis, while for the quadrotor with the new configuration, movement along the X-axis is prevented by the rotation of rotors in opposite directions along the y-axis attached to the body, as demonstrated in Fig. 9(b).

Fig. 9(a) shows the plots of angular velocities for rotors 1 and 3 in both quadrotors. The results shown in sub-plot (a) of this Fig., are analyzed similar to Fig. 7(a), with the difference that this time, the rotations are made about the y-axis.

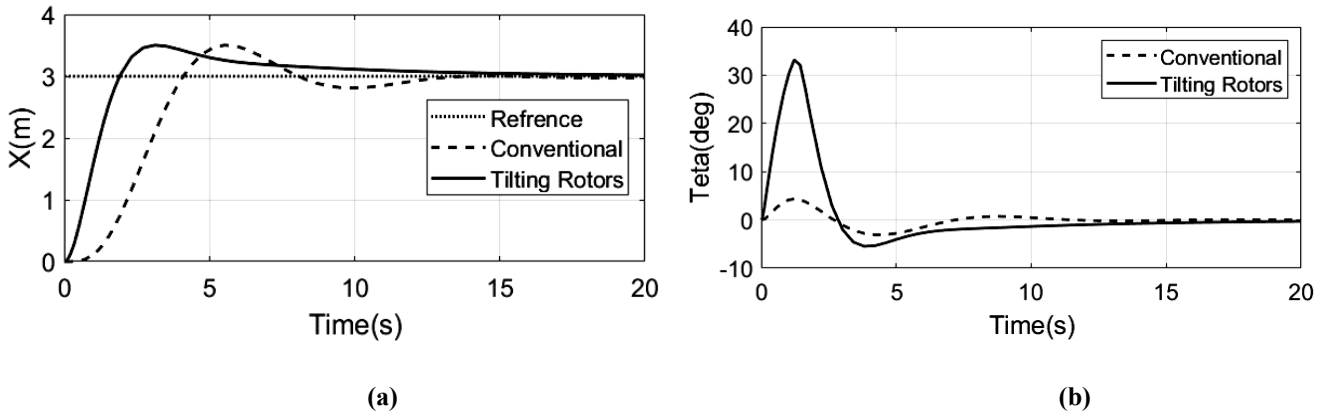

(a) **(b)**

Fig. 10. Diagrams of angular and linear positions along and X for underactuated and fully-actuated quadrotors for following a step in θ while the other degrees have zero references. (a) Linear position of X versus time, (b) Angular position of θ versus time.

5- 5- Tracking a step reference for the X position

The diagrams of position along the X-axis and the angle θ with respect to time are plotted in Fig. 10(a) and (b), respectively. From the subplot (a) of this Fig., the step input response for the position along the X-axis is more convenient than the results for the conventional quadrotor due to direct control of this output. In the conventional quadrotor, in order to control the motion along the X-axis, first a reference must be defined for the angle θ. The ability of the system to track the step reference for this position is limited to the ability of the controller of the angle θ in tracking the reference trajectory calculated for this angle. In this configuration, the response of the system to the input along the X-axis is significantly different from the response of the proposed configuration, due to the use of proportional-derivative controller and the limitations of this controller in tracking different reference functions.

In subplot (b) of Fig. 10, θ is plotted with respect to time, where the value of θ is much higher for the fully-actuated quadrotor, compared to the conventional quadrotor. The reason for this is the heights of the rotors from center of gravity in this configuration. The existence of this height causes the angle θ_{aR}, i.e., the lift force component generated along the x-axis of the quadrotor, to generate a torque about the y-axis attached to the body, due to the rotation of the rotors about this axis. Since the angles of all rotors, ϕ_{aR}, and θ_{aR}, are equal, this torque will have the same direction for all rotors. Therefore, it is necessary to compensate for this effect by creating a difference in rotors' angular velocities, which in turn creates differences in the torques generated by the vertical components of their lift forces about the y-axis attached to the body. Due to the constraints on the rotor speed, this difference is not fully applied at the beginning of the motion, Fig. 11(a), and as a result the quadrotor deviates around the y-axis attached to the body. The higher the height of the rotors relative to the center of gravity, the bigger this deviation will become. Therefore, performance of the fully-actuated quadrotor in separating linear and angular motions, is greatly affected by the height of the rotors relative to the center of gravity. For this reason, the height of the rotors has been reduced to 0.038 m. Of course, this issue can be resolved by eliminating the speed constraints or reducing the reference input for the position along the x-axis by 2 meters. Moreover, changing the control coefficients of the controller of the position along the X axis, can reduce this deviation.

Fig. 11(a) and (b) show the speeds of rotors 1 and 3 for both quadrotors, and the angles of rotors in the new configuration with respect to time, respectively. It can be seen from subplot (a) of this Figure that during the first 1 second of the movement, the summation of rotor speeds is higher for the new quadrotor configuration. The main reason of this issue, is the reduction of the vertical component of the lift force due to the quadrotor deviation along the angle θ and the increase of rotor speed to overcome the weight. Moreover, it can be seen that the speeds of rotors 1 and 3 are significantly different at the beginning of their movement. This is due to the need to overcome the torque resulting from the horizontal component of lift forces around the angle θ. As explained earlier, this torque is generated due to the height of rotors relative to the center of gravity. Also, it can be seen from subplot (b) that the angles of all rotors, are always equal to zero along the x-axis attached to the rotor; while the angle along the y-axis attached to the body is not equal to zero at the beginning and converges to zero over time. The reason for this issue is the need for the rotors to be angled at the beginning of their movement in order to create a lift force component along the X-axis and to accelerate the quadrotor along this axis. Eventually, and after achieving the desired tracking error along the X-axis, the rotors' are no longer required to rotate and the angle along the y-axis attached to the body gradually tends to zero.

To demonstrate the effects of rotors' height relative to the center of gravity in the fully-actuated quadrotor, step tracking curve for position of X is again presented in Fig. 12(a) and (b) for conventional and fully-actuated quadrotors, considering zero height for the rotors. It is clear from this Fig. that the

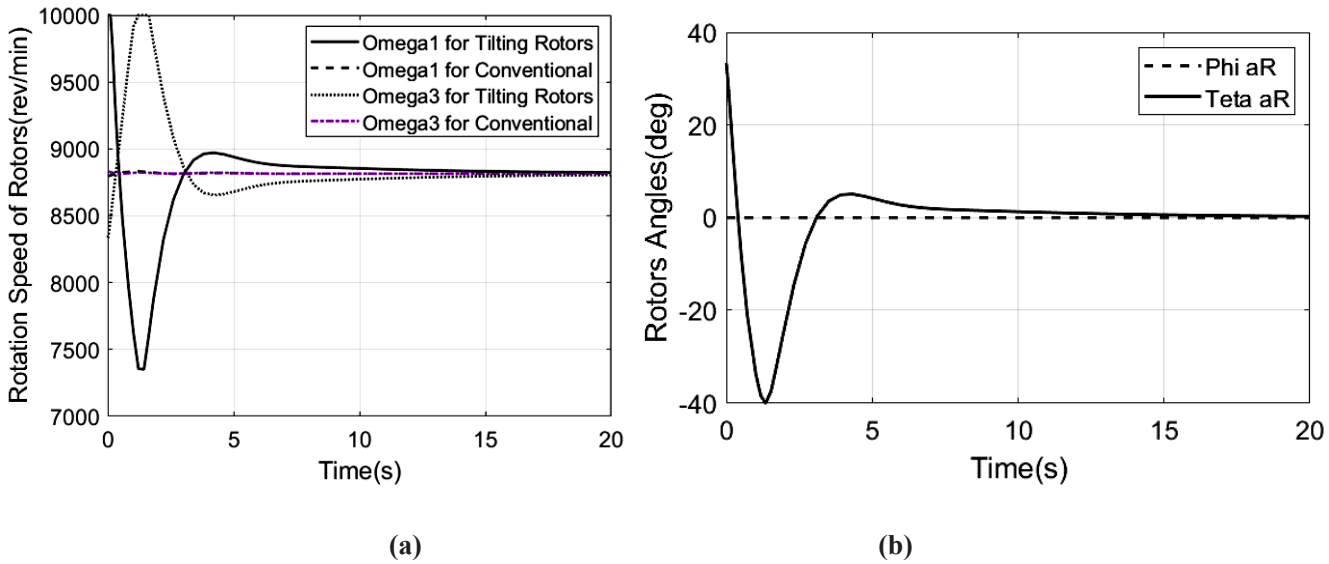

(a) **(b)**

Fig. 11. Diagrams of angular velocities for underactuated and fully-actuated quadrotors and plots of angles of the rotors for the fully-actuated quadrotor to follow a step in X while the other degrees have zero references. (a) Angular velocities versus time, (b) Rotors angles for the new configuration versus time.

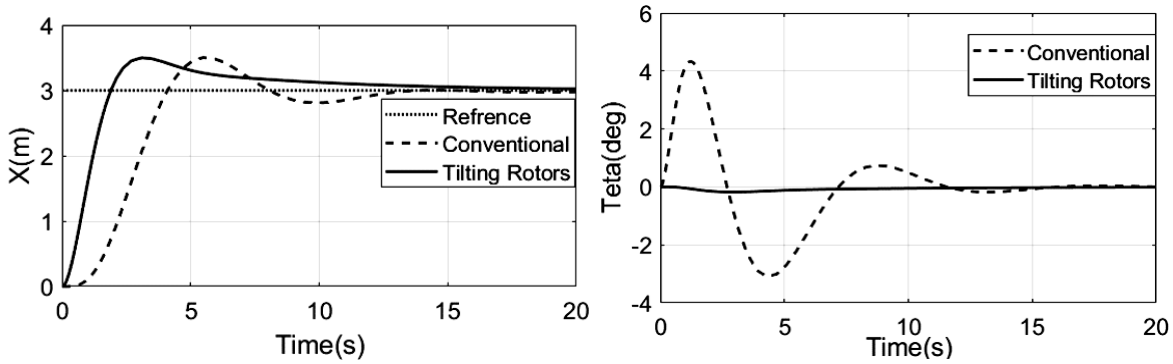

(a) **(b)**

Fig. 12. Diagrams of angular and linear positions along X and θ for underactuated and fully-actuated quadrotors for following a step in cX while the other degrees have zero references. (a) Linear position of X versus time, (b) Angular position of θ versus time.

diagram of the angle θ with respect to time is approximately zero for the fully-actuated quadrotor. The reason for the slight deviation of this angle in the fully-actuated quadrotor, is the torque applied from the rotors to the body, which results from the change in size and direction of angular motion.

Fig. 12(b) shows that the angle θ for the conventional quadrotor is much larger than its counterpart in the new configuration. As stated before, to move the quadrotor along the X-axis, the quadrotor needs to accelerate along this axis, so a force has to be applied to it in this direction. In the conventional quadrotor, this was achieved by the rotation of the quadrotor along the θ axis and generation of a lift force component along the X-axis; while in the new configuration, rotation of the rotors along the y-axis and creation of a lift force component along the X-axis, instead of rotation of the whole body, satisfies this maneuver. Therefore, there is no need for the rotation of the body in the new configuration.

5- 6- Tracking a step reference for the Y position

The diagrams of the positions along the Y-axis and the angle of ϕ with respect to time, are presented in Fig. 13(a) and (b), respectively.

The results of the diagrams shown in this Fig., are similar to step function tracking for position along the X-axis, except

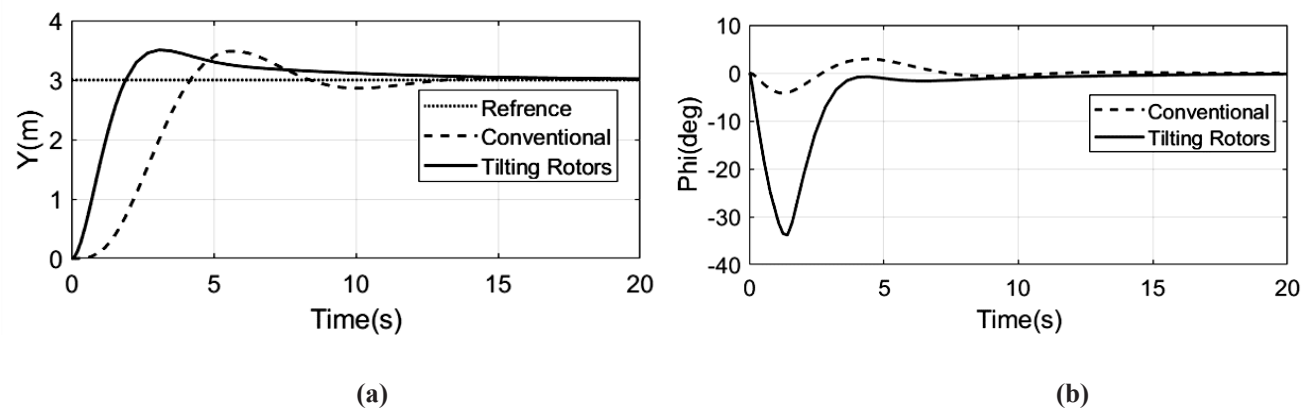

(a) (b)

Fig. 13. Diagrams of angular and linear positions along Y and ϕ for underactuated and fully-actuated quadrotors for following a step in ϕ while the other degrees have zero references. (a) Linear position of Y versus time, (b) Angular position of versus time.

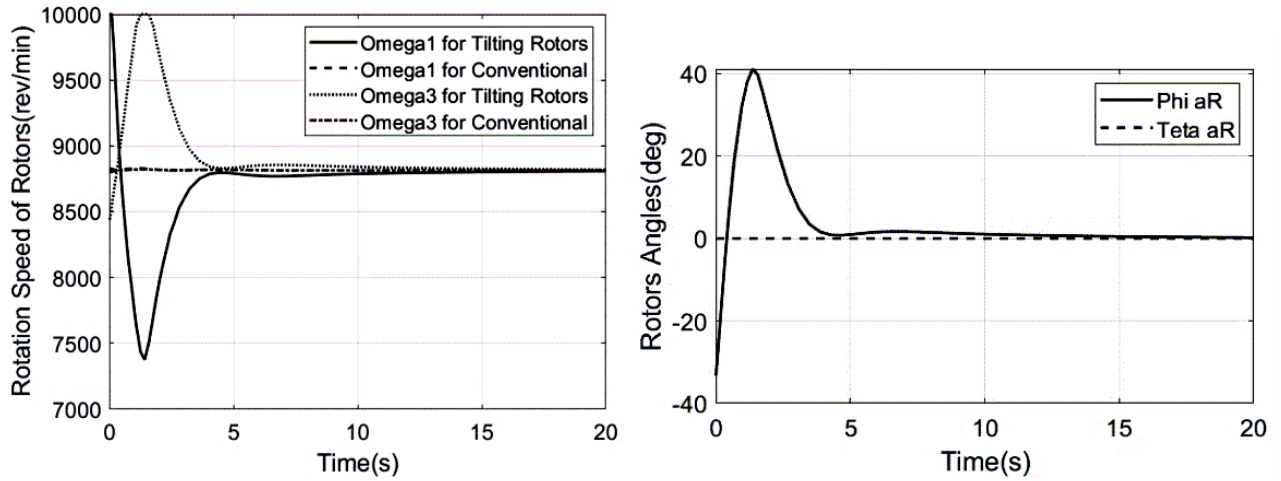

(a) (b)

Fig. 14. Diagrams of angular velocities for underactuated and fully-actuated quadrotors and plots of angles of the rotors for the fully-actuated quadrotor to follow a step in Y while the other degrees have zero references. (a) Angular velocities versus time, (b) Rotors angles for the new configuration versus time.

that in this case to track a step function along the Y-axis, the body and the rotors are required to deviate along the x-axis, the angle ϕ, for both conventional and new quadrotor configurations. Moreover, for reasons similar to the what was mentioned in the motion analysis along the X-axis, changes in the angle ϕ in the new configuration are higher than their counterparts in the conventional quadrotor, and similarly in this case, a reduction in the heights of rotors with respect to center of gravity, will reduce the deviation of the angle ϕ.

Fig. 14(a) and (b) present the speed diagrams of rotors 1 and 3 for both quadrotors and the rotor angles for the new configuration, with respect to time, respectively. The results obtained from this section are analyzed similar to those obtained for reference tracking along the X-axis.

5- 7- Tracking performance of the new configuration for different paths

In this part, four 3-dimensional reference trajectories are given to the quadrotor with the new configuration. Reference input functions are presented for locations along the X, Y and Z axes with respect to time. The reference values of the angles are assumed as either step or zero inputs. Further details are provided below for each path. The simulations are performed within the Simulink environment by applying a back-stepping nonlinear controller. The control gains applied for all paths are in accordance with Table 4, and the maximum speed allowed for the rotors is also equal to 12000 rpm.

Similar to the previous part, the effects of rotor disturbances are not considered in the design of nonlinear controller and does not create any significant impact on the

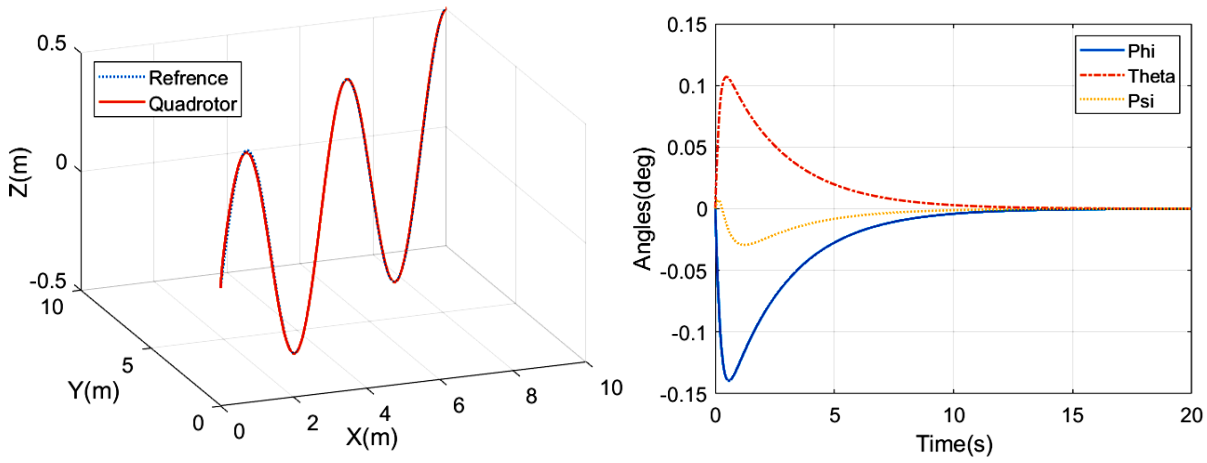

(a) **(b)**

Fig. 15. Diagrams of the 1st tracked path and the angles of the fully-actuated quadrotor using a back-stepping controller (a) Angular velocities versus time, (b) Fully-actuated quadrotor angles versus time.

results, due to the small values of $\dot{\theta}_{aR}$, $\dot{\phi}_{aR}$, $\ddot{\theta}_{aR}$, and $\ddot{\phi}_{aR}$, and the very small values of the moments of inertia of the rotors compared to the moment of inertia of the quadrotor's body.

First path

The functions X, Y, and Z with respect to time are presented in Eqs. (56)-(58).

$$X = v_x t \tag{56}$$

$$Y = v_y t \tag{57}$$

$$Z = A\sin\left(\sqrt{v_x^2 + v_y^2}\,t\right) \tag{58}$$

In these equations, v_x, v_y, and A are equal to 0.5 and the arbitrary values of the angles for this path are assumed to be equal to zero.

Fig. 15(a) and (b) present the diagram of the paths traveled by the quadrotor and the angles with respect to time, respectively. The diagram of angular velocity and the angles of the rotor are also plotted in Fig. 16(a) and (b).

As can be seen from these Fig.s, the quadrotor has tracked the related trajectory, however the angles ϕ and θ suffer from a slight deviation. The reason for this is that the angular velocities of the rotors are limited and on the other hand, their values are required to be higher at the beginning of the motion in order to maintain the angles at zero. In other words, the angular velocities of the rotors are smaller than the values required to maintain the angles at zero at the beginning of the motion. Therefore, the angles deviate from zero at the beginning; but over time and with the application of the next control inputs, they return to equilibrium. The angles of all rotors, ϕ_{aR}, and θ_{aR}, slightly rotate at the beginning but tend to zero after a while. The reason for this is the definition of motion along the X and Y axes as a constant velocity and the lack of accelerations along these two axes. Therefore, to prevent the rotation of the quadrotor along ϕ and θ, the rotors slightly rotate at the beginning of the motion so that the lift component generated along the X and Y axes, accelerates the quadrotor along them. After a short time and when the quadrotor reaches its desired speed along these two axes, the rotors return to their previous state, the zero angle. If the friction due to air resistance is taken into consideration, there exists wind flow, or the motion is defined as accelerated in one of the X or Y axes, then the pattern for the diagram of these angles will change. The third point is demonstrated for the next path. Another important point is that the greater the curvature of the path, and the larger the amplitude or the frequency, the greater the deviation of the angles ϕ and θ from zero will become.

Second path

The general pattern of this path is similar to the first one, except that in this path the motion along the Y-axis is sinusoidal while the motion along the X and Z axes are linear. The equations for this motion are expressed as follows.

$$X = v_x t \tag{59}$$

$$Y = A\sin\left(\sqrt{v_x^2 + v_z^2}\,t\right) \tag{60}$$

$$Z = v_z t \tag{61}$$

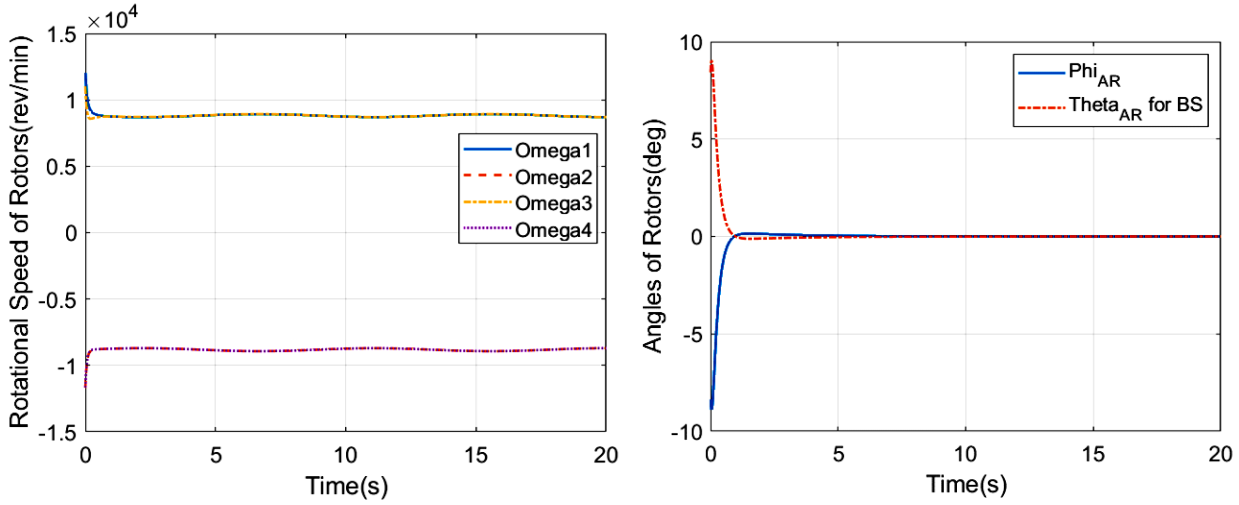

(a) (b)

Fig. 16. Diagrams of the 1st tracked path of the new configuration using a back-stepping controller (a) Angular velocities versus time, (b) Fully-actuated quadrotor angles versus time.

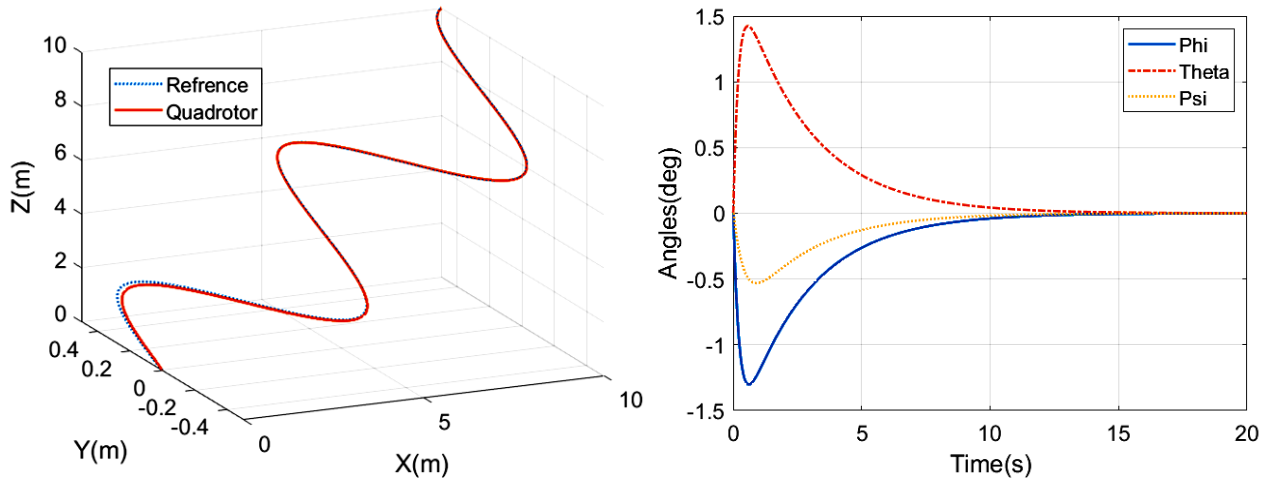

(a) (b)

Fig. 17. Diagrams of the tracked path and the angles of the fully-actuated quadrotor by a back-stepping controller (a) 2nd tracked path versus time, (b) Fully-actuated quadrotor angles versus time.

where the values of v_x, v_z, and A are assumed equal to 0.5. The tracking path and angles of the quadrotor with respect to time are presented in Fig. 17(a) and (b). The analysis of these diagrams is similar to the previous case. The tracking is performed well and the angles slightly deviated from their desired values at the beginning of the motion, due to the limitations of the rotors' speed.

In this path, due to the sinusoidal nature of the Y function with respect to time, as seen in Fig. 18(b), the trajectory of ϕ_{aR} with respect to time, becomes sinusoidal, and unlike the previous path, does not converge to zero after a while. Whereas, the trajectory of θ_{aR} with respect to time gradually tends to zero due to the linear equation of the motion along the X axis.

Third path

The kinetic equations of the third path along the Y, X, and Z axes are similar to the first path. These are presented in Eqs. (56)-(58). The reference values for the angles ϕ and θ along this path, are 45°, while the arbitrary value of ψ is assumed equal to zero. The path and angles trajectories are presented in Fig. 19(a) and (b), respectively, while Fig. 20(a) and (b) present the angular velocities and angles of the rotors with respect to time.

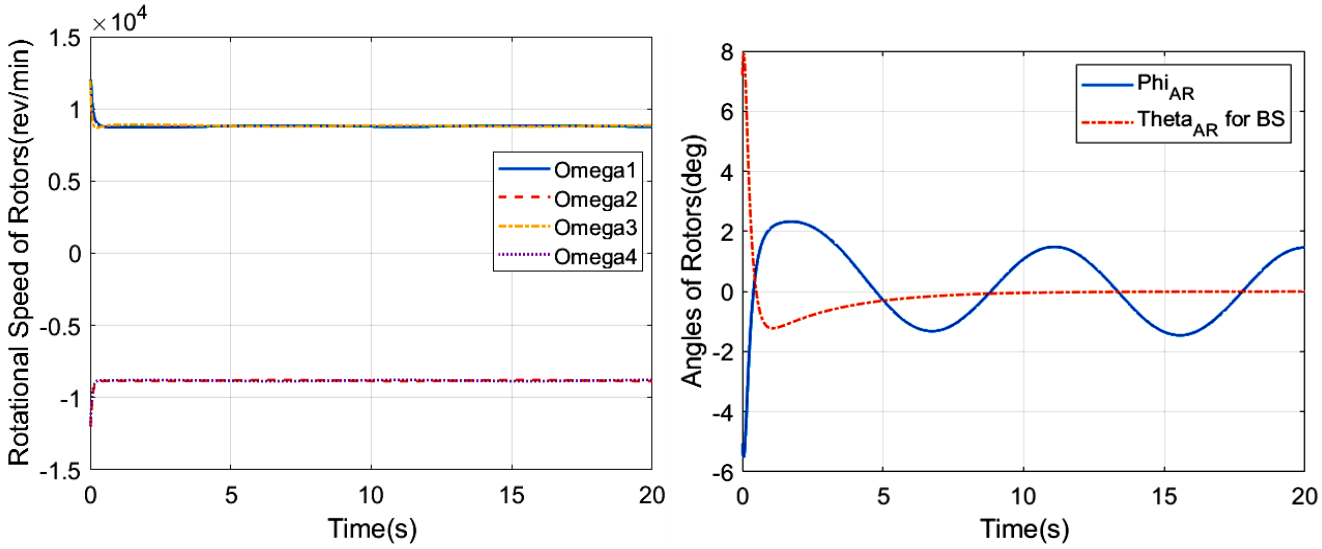

(a) (b)

Fig. 18. Diagrams of the 2nd tracked path of the new configuration using a back-stepping controller (a) Angular velocities versus time, (b) Fully-actuated quadrotor angles versus time.

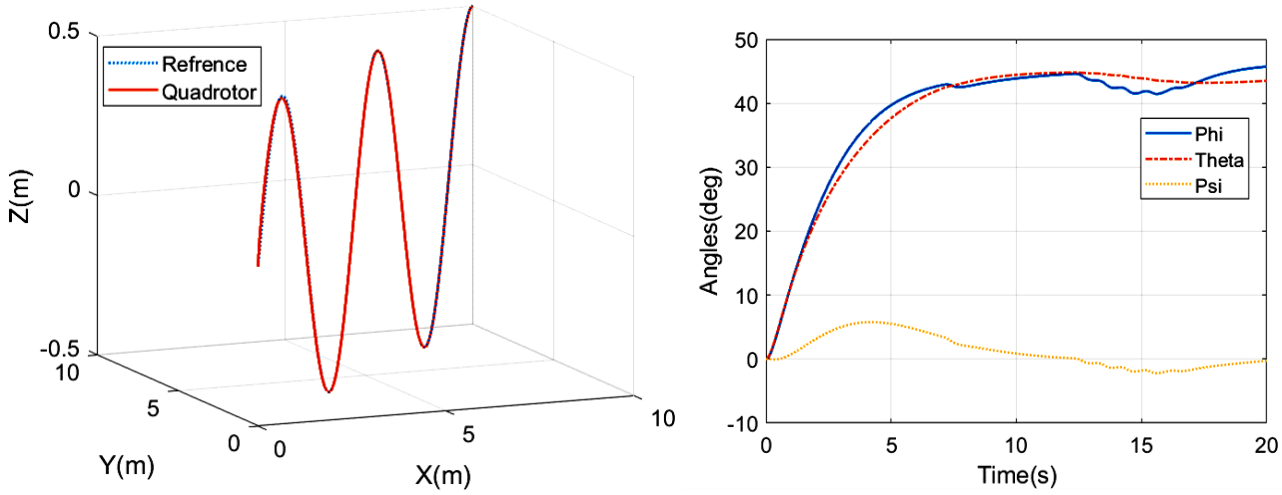

(a) (b)

Fig. 19: Diagrams of the tracked path and the angles of the fully-actuated quadrotor by a back-stepping controller (a) 3rd tracked path versus time, (b) New quadrotor angles versus time.

As observed in these Fig.s, the path tracking is satisfactory, however tracking the angles is accompanied by errors and oscillations. The value of this error for the angle ψ is 2.3 degrees and it is equal to 4 and 8 percent for the angles ϕ and θ, respectively. This is due to the limitations on the rotor speeds, the disturbances resulting from the torque applied by the rotors to the body and the priority of following the X and Y locations over the angles while transforming virtual control inputs to rotors' speeds and angles. As seen from Fig. 20(a), one of the rotors always operates in saturation and thus the quadrotor is not capable of stabilizing its angles. It should be noted that the limitation observed in this configuration is a limitation of actuators rather than a structural (kinematic) constraint.

Fourth path

This path is similar to the second path, however the arbitrary values of ϕ and θ are assumed as a step function with the value of 45°. The equations of X, Y, and Z are presented in Eqs. (59) – (61). The subplots (a) and (b) of Figs. (21) and (22), present the diagrams of the paths, quadrotor angles, rotor speeds and rotor angles, respectively.

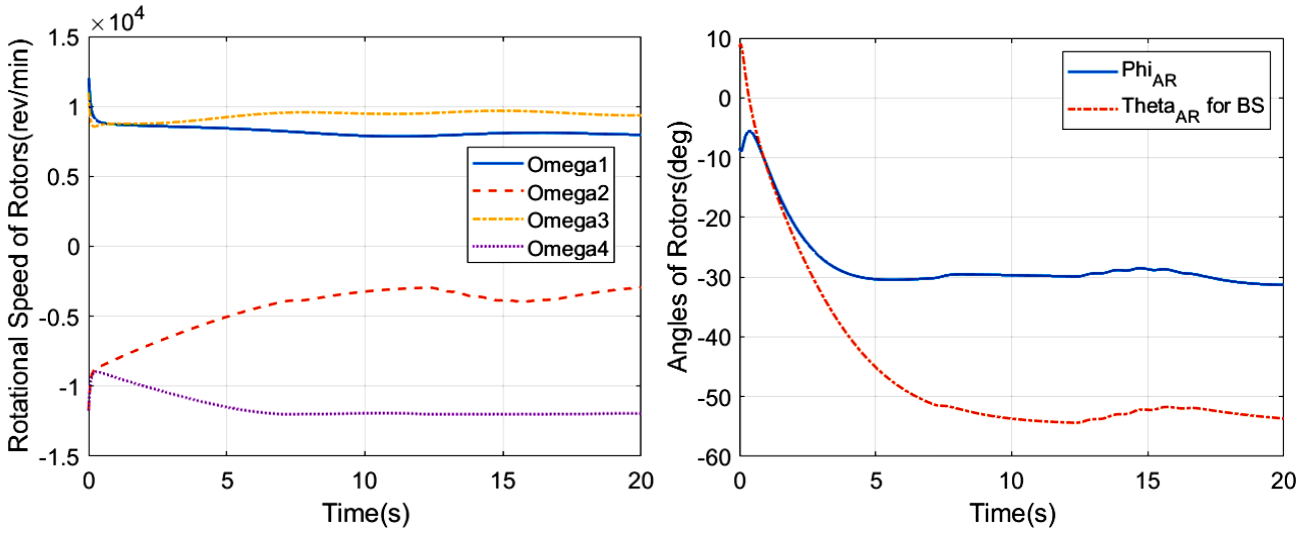

(a) (b)

Fig. 20. Diagrams of the 3rd tracked path of the new configuration using a back-stepping controller (a) Angular velocities versus time, (b) Fully-actuated quadrotor angles versus time.

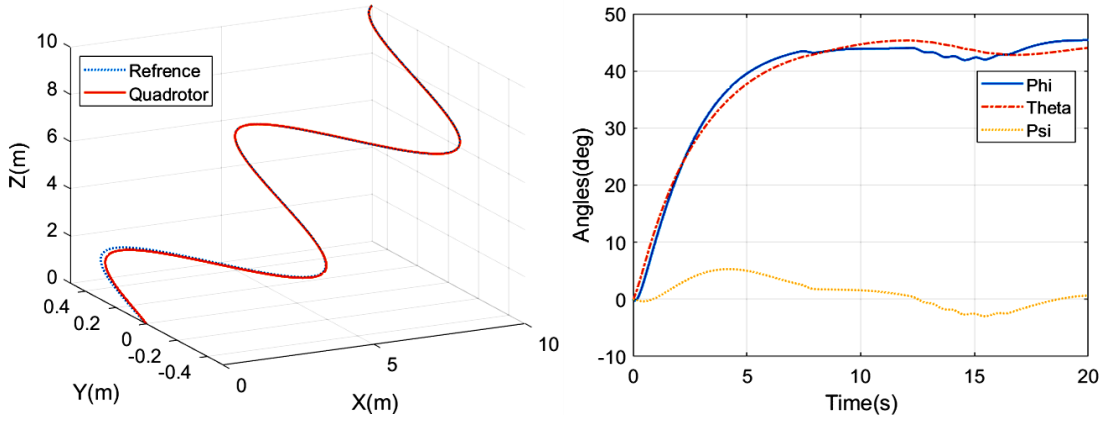

(a) (b)

Fig. 21. Diagrams of the tracked path and the angles of the fully-actuated quadrotor by a back-stepping controller (a) 4th tracked path versus time, (b) New quadrotor angles versus time.

The analyzes of this path are similar to the analyzes presented for the third path. The path is still well-tracked, while the tracking of the angles is weak and along with oscillations. The error value for the angle ψ is equal to 3 degrees, and equal to 7 and 5 percent for the angles ϕ and θ, respectively. As explained, the reason for this is the saturation of a number of actuators and the disturbances resulting from the torque applied to the body by the rotors. It is observed that due to the imbalance of the quadrotor angles' diagram, the pattern of rotor angles is no longer sinusoidal and is accompanied by oscillations.

6- Conclusions and future works

In this article, first a quadrotor with a new configuration was introduced. The aim of proposing this novel configuration was to increase the number of controllable degrees of freedom from 4 to 6 and to eliminate the motion couplings. The introduced configuration was such that all rotors were able to rotate simultaneously and with equal values, along the two directions of the x-axes attached to the rotors and the y axis attached to the quadrotor's body.

The equations governing this configuration were extracted after some simplifying assumptions using the Newton-Euler

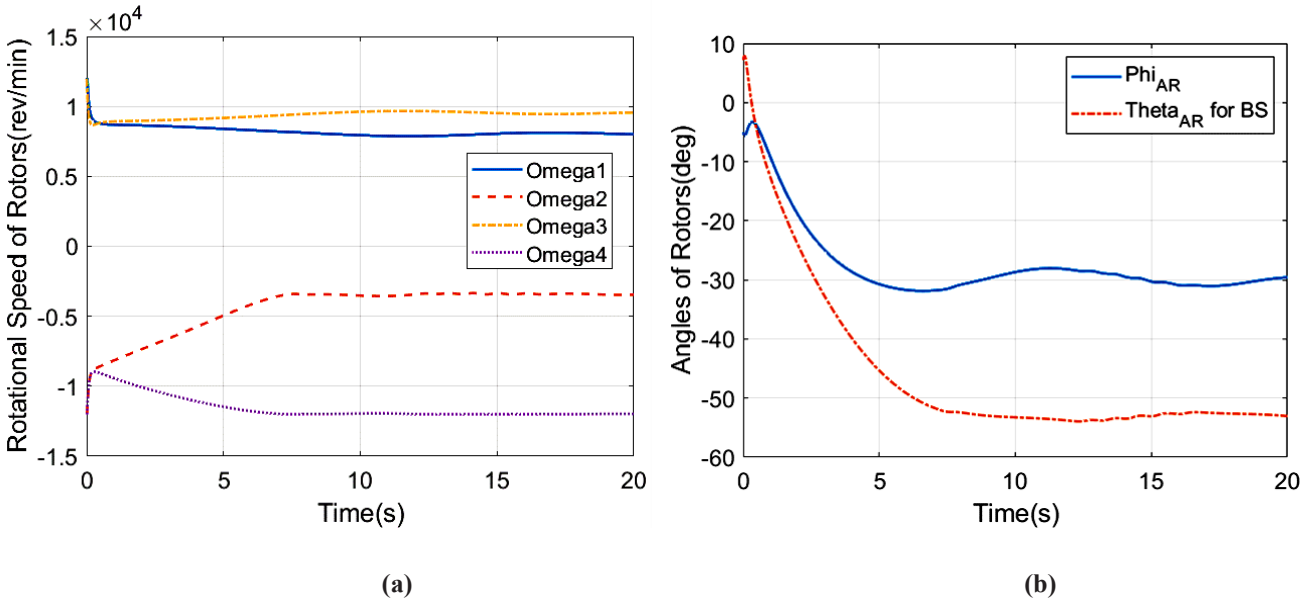

Fig. 22. Diagrams of the 4th tracked path of the new configuration using a back-stepping controller (a) Angular velocities versus time, (b) Fully-actuated quadrotor angles versus time.

method. A controller was then designed for this quadrotor. To determine the motion capabilities of this quadrotor, a proportional-derivative controller was first designed to control the positions and angles, after linearization about the origin. In the next step, a nonlinear controller was designed using the back-stepping method, and the stability of the system under the designed controller was proved by designing a Lyapunov function.

In the final section, the simulation results obtained from Simulink software environment were presented and analyzed. For this purpose, first the kinetic capabilities of the conventional quadrotor were compared to the new configuration. Angular speed saturation for the actuators was considered on 10000 rpm and tilting angle of the rotors around body frame's X axis on $80°$. The results showed that the new configuration is capable of eliminating motion couplings between linear and angular motions in tracking a step function for the angles ϕ and θ. The linear controller is manually tuned for that the tracking overshoot remains beyond 17% and the rise time reduces as well. It was found during the tracking of the step function for X and Y positions that the ability of the new configuration to eliminate the motion coupling between positions and angles, strongly depends on the height of the rotors relative to the quadrotor's center of gravity, and the reduction of height in this configuration, significantly increases this ability. In the rest of this section, four reference paths which are usual for aerial motions were separately applied to determine the abilities and limitations of the motions of the quadrotor with the new configuration. Since a linear controller for this system is not trustable, a nonlinear back-stepping controller is applied for trajectory tracking. The results showed that, due to the limitations on the actuators, the motion couplings between the degrees of freedom were not completely eliminated and the quadrotor was not able to perfectly track the reference values for the angles. However, tracking of the complex trajectories was acceptable and if the nonlinear controller is used, the new proposed configuration for the quadrotor is capable of overcoming motion couplings and controlling all 6 degrees of freedom.

In future works, various maneuvers will be applied into the fully-actuated quadrotor and the capabilities and limitations of this quadrotor can be more precisely identified. Also due to necessary characteristics of quadrotors during formation flight, this quadrotor will be investigated for leader – follower formation for load transportation.

References

[1] I.B. Viana, D.A. dos Santos, L.C.S. Góes, Formation control of multirotor aerial vehicles using decentralized MPC, Journal of the Brazilian society of mechanical sciences and engineering, 40 (2018) 1-12.

[2] H. Kiaee, H. Heidari, Cooperative path planning for leader–follower formation of Multi UAV based on the minimum energy consumption for load transportation, Amirkabir Journal of Mechanical Engineering, 52(12) (2019) 3327-40.

[3] H. Heydari, Optimal Trajectory Planning of a Quadrotor Based on Minimum Effort, Amirkabir Journal of Mechanical Engineering, 51(1) (2019) 169-79.

[4] T. Omar, M.L. Nehdi, Remote sensing of concrete bridge decks using unmanned aerial vehicle infrared thermography, Automation in Construction, 83 (2017)

360-371.

[5] M. Becker, R.C.B Sampaio, S. Bouabdallah, V. Perrot, R. Siegwart, In flight collision avoidance for a Mini-UAV robot based on onboard sensors, Journal of the Brazilian society of mechanical sciences and engineering, 2(12) 2012.

[6] J. Zhang, J. Hu, J. Lian, Z. Fan, X. Ouyang, W. Ye, Seeing the forest from drones: Testing the potential of lightweight drones as a tool for long-term forest monitoring, Biological Conservation, 198 (2016) 60-69.

[7] A. Hernandez, H. Murcia, C. Copot, R. De Keyser, Towards the development of a smart flying sensor: illustration in the field of precision agriculture, Sensors, 15(7) (2015) 16688-16709.

[8] Z. Lu, F. Nagata, K. Watanabe, M.K. Habib, iOS application for quadrotor remote control, Artificial Life and Robotics, 22 (2017) 374-379.

[9] Z. Lu, F. Nagata, K. Watanabe, Mission planning of iOS application for a quadrotor UAV, Artificial Life and Robotics, 23 (2018) 428-433.

[10] E. Cetinsoy, S. Dikyar, C. Hancer, K. Oner, E. Sirimoglu, M. Unel, M. Aksit, Design and construction of a novel quad tilt-wing UAV, Mechatronics, 22(6) (2012) 723-745.

[11]] M. Zhao, T. Anzai, F. Shi, X. Chen, K. Okada, M. Inaba, Design, modeling, and control of an aerial robot dragon: A dual-rotor-embedded multilink robot with the ability of multi-degree-of-freedom aerial transformation, IEEE Robotics and Automation Letters, 3(2) (2018) 1176-1183.

[12] D. Falanga, K. Kleber, S. Mintchev, D. Floreano, D. Scaramuzza, The foldable drone: A morphing quadrotor that can squeeze and fly, IEEE Robotics and Automation Letters, 4(2) (2019) 209-216.

[13] M. Navabi, A. Davoodi, H. Mirzaei, Trajectory tracking of under-actuated quadcopter using Lyapunov-based optimum adaptive controller, Proceedings of the Institution of Mechanical Engineers, Part G: Journal of Aerospace Engineering, 236(1) (2022) 202-215.

[14] H. Jokar, R. Vatankhah, Adaptive fuzzy global fast terminal sliding mode control of an over-actuated flying robot, Journal of the Brazilian society of mechanical sciences and engineering, 42 (2020) 1-18.

[15] A. Alkamachi, E. Ercelebi, Modelling and control of H-shaped racing quadcopter with tilting propellers, Facta Universitatis, Series: Mechanical Engineering, 15(2) (2017) 201-215.

[16] Y. Nakamura, A. Arakawa, K. Watanabe, I. Nagai, An improvement of flight performance in the level flight of tilted quadrotors by attaching a fixed-wing, Artificial Life and Robotics, 24 (2019) 396-403.

[17] M. Kamel, S. Verling, O. Elkhatib, C. Sprecher, P. Wulkop, Z. Taylor, R. Siegwart, I. Gilitschenski, Voliro: An omnidirectional hexacopter with tiltable rotors, arXiv, 2018.

[18] S. Badr, O. Mehrez, A. Kabeel, A novel modification for a quadrotor design, International Conference on Unmanned Aircraft Systems (ICUAS), 2016, pp. 702-710.

[19] M. Cutler, J.P. How, Analysis and control of a variable-pitch quadrotor for agile flight, Journal of Dynamic Systems, Measurement, and Control, 137(10) (2015).

[20] F. Senkul, E. Altug, Modeling and control of a novel tiltRoll rotor quadrotor UAV, International Conference on Unmanned Aircraft Systems (ICUAS), 2013, pp. 1071-1076.

[21] M. Elfeky, M. Elshafei, A.W.A. Saif, M.F. Al-Malki, Quadrotor helicopter with tilting rotors: Modeling and simulation, World congress on computer and information technology (WCCIT), 2013, pp. 1-5.

[22] N.D.S Fernandes, Design and construction of a multi-rotor with various degrees of freedom, M.Sc. Thesis, Lisbon University, 2011.

[23] X. Xu, K. Watanabe, I. Nagai, Feedback linearization control for a tandem rotor UAV robot equipped with two 2-DOF tiltable coaxial-rotors, Artificial Life and Robotics, 26 (2020) 259-268.

[24] M.W. Spong, S. Hutchinson, M. Vidyasagar, Robot Modeling and Control, Hoboken, NJ: John Wiley & Sons, 2006.

[25] G. Nandakumar, T. Ranganathan, B.A. Arjun, A. Thondiyath, Design and analysis of a novel quadrotor system-VOOPS, IEEE International Conference on Robotics and Automation (ICRA), 2015, pp. 1692-1697.

[26] Y. Naidoo, R. Stopforth, G. Bright, Quad-Rotor unmanned aerial vehicle helicopter modelling & control, International Journal of Advanced Robotic Systems, 8(4) (2011).

[27] Y. Aslani Darandashi, Modification of the multi-rotors mechanical structure and design of a suitable controller for increase of stability & maneuverability, M.Sc thesis, Amirkabir University of Technology, 2020.

HOW TO CITE THIS ARTICLE

Y. Aslani Darandashi, R. Fesharakifard, A. Ohadi, Investigation on performance improvement of a fully-actuated quadrotor, AUT J. Mech Eng., 7(1) (2023) 19-40.

DOI: 10.22060/ajme.2022.21384.6034